Mon. Not. R. Astron. Soc. **388,** 1223–1238 (2008) doi:10.1111/j.1365-2966.2008.13430.x

# Magnetorotational instability in protoplanetary discs: the effect of dust grains

Raquel Salmeron[1,2]⋆ and Mark Wardle[3]

[1]*Planetary Science Institute, Research School of Astronomy and Astrophysics and Research School of Earth Sciences, Australian National University, Canberra ACT 2611, Australia*
[2]*Department of Astronomy and Astrophysics, The University of Chicago, Chicago, IL 60637, USA*
[3]*Department of Physics, Macquarie University, Sydney NSW 2109, Australia*

Accepted 2008 May 7. Received 2008 April 18; in original form 2008 January 15

**ABSTRACT**

We investigate the linear growth and vertical structure of the magnetorotational instability (MRI) in weakly ionized, stratified protoplanetary discs. The magnetic field is initially vertical and dust grains are assumed to be well mixed with the gas over the entire vertical dimension of the disc. For simplicity, all the grains are assumed to have the same radius ($a = 0.1, 1$ or 3 μm) and constitute a constant fraction (1 per cent) of the total mass of the gas. Solutions are obtained at representative radial locations ($R = 5$ and 10 au) from the central protostar for a minimum-mass solar nebula model and different choices of the initial magnetic field strength, configuration of the diffusivity tensor and grain sizes.

We find that when no grain are present, or they are $\gtrsim$1 μm in radius, the mid-plane of the disc remains magnetically coupled for field strengths up to a few gauss at both radii. In contrast, when a population of small grains ($a = 0.1$ μm) is mixed with the gas, the section of the disc within two tidal scaleheights from the mid-plane is magnetically inactive and only magnetic fields weaker than ∼50 mG can effectively couple to the fluid. At 5 au, Ohmic diffusion dominates for $z/H \lesssim 1$ when the field is relatively weak ($B \lesssim$ a few milligauss), irrespective of the properties of the grain population. Conversely, at 10 au this diffusion term is unimportant in all the scenarios studied here. High above the mid-plane ($z/H \gtrsim 5$), ambipolar diffusion is severe and prevents the field from coupling to the gas for all $B$. Hall diffusion is dominant for a wide range of field strengths at both radii when dust grains are present.

The growth rate, wavenumber and range of magnetic field strengths for which MRI-unstable modes exist are all drastically diminished when dust grains are present, particularly when they are small ($a \sim 0.1$ μm). In fact, MRI perturbations grow at 5 au (10 au) for $B \lesssim 160$ mG (130 mG) when 3 μm grains are mixed with the gas. This upper limit on the field strength is reduced to only ∼16 mG (10 mG) when the grain size is reduced to 0.1 μm. In contrast, when the grains are assumed to have settled, MRI-unstable modes are found for $B \lesssim 800$ mG at 5 au and 250 mG at 10 au. Similarly, as the typical size of the dust grains diminishes, the vertical extent of the dead zone increases, as expected. For 0.1 μm grains, the disc is magnetically inactive within two scaleheights of the mid-plane at both radii, but perturbations grow over the entire section of the disc for grain sizes of 1 μm or larger. When dust grains are mixed with the gas, perturbations that incorporate Hall diffusion grow faster, and are active over a more extended cross-section of the disc, than those obtained under the ambipolar diffusion approximation.

Note that the stabilizing effect of small dust grains (e.g. $a = 0.1$ μm) is not strong enough to completely suppress the perturbations. We find, in fact, that even in this scenario, the magnetic field is able to couple to the gas and shear over a range of fluid conditions. Despite the

⋆E-mail: raquel@mso.anu.edu.au

low-magnetic coupling, MRI modes grow for a range of magnetic field strengths and Hall diffusion largely determines the properties of the perturbations in the inner regions of the disc.

**Key words:** accretion, accretion discs – instabilities – MHD – stars: formation.

## 1 INTRODUCTION

Magnetic fields may regulate the 'disc accretion phase' of star formation by providing means of transporting away the excess angular momentum of the disc, enabling matter to accrete. The more generally relevant mechanisms associated with this are magnetohydrodynamic (MHD) turbulence induced by the magnetorotational instability (MRI; Balbus & Hawley 1991, 1998) and outflows driven centrifugally from the disc surfaces (Blandford & Payne 1982, hereafter BP82; Wardle & Königl 1993; see also the review by Königl & Pudritz 2000). These processes are, in turn, thought to play key roles in the dynamics and evolution of astrophysical accretion discs. Magnetically driven turbulence is likely to impact disc chemistry (e.g. Ilgner & Nelson 2006; Semenov, Wiebe & Henning 2006) as well as the properties – and evolution – of dust grains mixed with the gas (e.g. Turner et al. 2006). Magnetic resonances have been shown to modify the net tidal torque exerted by the disc on a forming planet and thus, alter the speed and direction of the planet's migration through the disc (Terquem 2003; Johnson, Goodman & Menou 2006). Finally, the magnetically inactive (dead) zones (Gammie 1996; Wardle 1997) are not only the regions where planets are thought to form, but also they have been invoked as a possible mechanism to stop their inward migration (e.g. Matsumura & Pudritz 2005).

In protoplanetary discs, however, the magnetic diffusivity can be high enough to limit – or even suppress – these processes. The specific role magnetic fields are able to play in these environments is, therefore, largely determined by the degree of coupling between the field and the neutral gas. A critical parameter for this analysis is the ionization fraction of the fluid, which reflects the equilibrium between ionization and recombination processes taking place in the disc. Ionization processes outside the disc innermost sections ($R \gtrsim 0.1$ au) are non-thermal, driven by interstellar cosmic rays, X-rays emitted by the magnetically active protostar and radioactive decay (Hayashi 1981; Glassgold, Najita & Igea 1997; Igea & Glassgold 1999; Fromang, Terquem & Balbus 2002). On the other hand, free electrons are lost through recombination processes which, in general, take place both in the gas phase and on grain surfaces (e.g. Nishi, Nakano & Umebayashi 1991).

Dust grains affect the level of magnetic coupling in protoplanetary discs when they are well mixed with the gas (e.g. in relatively early stages of accretion and/or when turbulence prevents them from settling towards the mid-plane). They do so in two ways. First, they reduce the ionization fraction by providing additional pathways for electrons and ions to recombine on their surfaces. Secondly, charged dust particles can become important species in high-density regions (Umebayashi & Nakano 1990; Nishi et al. 1991). For example, at 1 au in a disc where 0.1 μm grains are present, positively charged particles are the most abundant ionized species within two scaleheights from the mid-plane (see fig. 6 of Wardle 2007; hereafter W07). As these particles generally have large cross-sections, collisions with the neutrals are important and they become decoupled (or partially decoupled) to the magnetic field at densities for which smaller species, typically ions and electrons, would still be well tied to it.

Both of these mechanisms act to lower the conductivity of the fluid, especially near the mid-plane where the density is high and ionization processes are inefficient. In the minimum-mass solar nebula disc (Hayashi 1981; Hayashi, Nakasawa & Nakagawa 1985), for example, X-rays are completely attenuated below $z/H \sim 1.7$ (see fig. 1 of Salmeron & Wardle 2005, hereafter SW05). As a result, in the disc inner sections the magnetic coupling may be insufficient to provide adequate link between the neutral particles and the field. Moreover, recent calculations for a minimum-mass solar nebula disc exposed to X-ray and cosmic ray ionizing fluxes (W07) indicate that near the surface (above three to four tidal scaleheights) the magnetic diffusivity can also be severe, even though in these regions the ionizing flux is strongest and the electron fraction is significantly larger than it is in the disc interior. This effect results from the strong decline in the number density of charged particles high above the mid-plane. These considerations suggest that magnetic activity in the inner regions of weakly ionized discs may well be confined to intermediate heights above the mid-plane ($z/H \sim 2$–$4$).

It is clear that the level of magnetic diffusion is strongly dependent on the presence, and size distribution, of dust particles suspended in the gas phase. In fact, once dust grains have settled, the ionization fraction may be enough to produce adequate magnetic coupling over the entire vertical extension of the disc even at $R \lesssim 1$ au (W07). A realistic study of the properties of the MRI in these discs must, therefore, incorporate a consistent treatment of dust dynamics and evolution [unless they are assumed to have settled, a good approximation to model relatively late accretion stages, as was the case in Salmeron & Wardle (2003, hereafter SW03) and SW05]. This analysis is further complicated because dust grains have complex spatial and size distributions (e.g. Mathis, Rumpl & Nordsieck 1977; Umebayashi & Nakano 1990; D'Alessio et al. 2006), determined by the competing action of processes involving sticking, shattering, coagulation, growth (and/or sublimation) of ice mantles and settling to the mid-plane (e.g. Weidenschilling & Cuzzi 1993). Previous results also (SW03, SW05) highlight the importance of incorporating in these studies all three diffusion mechanisms between the magnetic field and the neutral fluid (namely, the Ohmic, Hall and Ambipolar diffusivities), as Hall diffusion largely determines the growth and structure of MRI perturbations, particularly in the disc inner regions (e.g. within distances of the order of a few au from the central protostar; SW05). This is implemented here via a diffusivity tensor formalism (Cowling 1957; Norman & Heyvaerts 1985; Nakano & Umebayashi 1986; Wardle & Ng 1999, W07).

Dust grains can affect the structure and dynamics of accretion discs via two additional mechanisms: dust opacity can modify the radiative transfer within the disc – which, in turn, can dramatically alter its structure – and dust particles may become dynamically important if their abundance is sufficiently high. In this study, both effects are small because the disc is vertically isothermal and grains constitute only a small fraction of the mass of the gas (see below).

In this paper, we study the vertical structure and linear growth of the MRI in a disc where dust grains are well mixed with the gas over its entire vertical dimension. Results are presented for two representative distances ($R = 5$ and 10 au) from the central protostar. For simplicity, we assume that all particles have the same

radius – $a = 0.1$, 1 or 3 μm – and constitute 1 per cent of the total mass of the gas, a typical assumption in studies of molecular clouds (Umebayashi & Nakano 1990). This fraction is constant with height, which means that we have also assumed that no sedimentation has occurred. Although this is a very simplified picture, the results illustrate the importance of dust particles in the delicate ionization equilibrium of discs, and consequently, on their magnetic activity.

The paper is organized as follows. The adopted disc model is described in Section 2. Section 3 briefly summarizes the formulation and methodology, which are based on SW05. We refer the reader to that study – and references therein – for further details (for the sake of clarity, the linearized equations are also reproduced in Appendix A). This section also includes a discussion of the typical dependence of the components of the diffusivity tensor and magnetic coupling with height with (and without) grains for the two radial positions of interest. Section 4 then presents the vertical structure and linear growth of MRI-unstable modes at these radii and compares solutions incorporating different diffusion mechanisms and assumptions regarding the presence, and size, of dust grains. These results, and possible implications for the dynamics and evolution of low-conductivity discs, are discussed in Section 5. Our main conclusions are summarized in Section 6.

## 2 DISC MODEL

Our fiducial disc, assumed to be geometrically thin and vertically isothermal, is based on the minimum-mass solar nebula model (Hayashi 1981; Hayashi et al. 1985). Our formulation incorporates the disc vertical stratification but – following common practice – it neglects radial gradients. This is appropriate, as these gradients typically occur over a much larger length-scale than those in the vertical direction. Under these assumptions, the equilibrium structure of the disc is the result of the balance between the vertical component of the gravitational force exerted by the central object and the pressure gradient within the disc. The vertical profile of the density is then given by

$$\frac{\rho(r,z)}{\rho_0(r)} = \exp\left[-\frac{z^2}{2H^2(r)}\right], \tag{1}$$

where $\rho_0$ is the mid-plane density and $H \equiv c_s/\Omega$ is the tidal scale-height of the gas. The neutral gas is assumed to be composed of molecular hydrogen and helium, such that $n_{He} = 0.2\, n_{H_2}$, which results in $n_H(r,z) = \rho(r,z)/1.4\, m_H$.

As already mentioned above, a key feature of protoplanetary accretion discs is that they are weakly ionized. This is because ionization processes are generally ineffective (except possibly in the vicinity of the star and in the surface regions), while the recombination rate is accelerated by the high density of the fluid and the removal of charges by dust grains (if present). In fact, outside the innermost 0.1–0.3 au, where thermal effects are relevant (e.g. Hayashi 1981), the main ionizing sources are X-rays and ultraviolet (UV) radiation emanating from the central object (e.g. Glassgold, Feigelson & Montmerle 2000) and – to a much lesser extent – the decay of radioactive materials, particularly $^{40}$K (Consolmagno & Jokipii 1978; Sano et al. 2000). Interstellar cosmic rays may also be important as they can potentially reach deeper into the disc than X-ray and UV fluxes do. In fact, cosmic rays are the dominant ionizing source at 1 au for $z/H \lesssim 2.2$ (they even reach the mid-plane at this radius, albeit significantly attenuated; e.g. SW05). However, their actual contribution is unclear because the low-energy particles responsible for ionization may be scattered by outflows launched from the protostar-disc system (e.g. Fromang et al. 2002). On the other hand, recombination processes in the disc generally occur both in the gas phase (through the dissociative recombination of electrons with molecular ions and the radiative recombination with metal ions) and on grain surfaces (e.g. Oppenheimer & Dalgarno 1974; Spitzer 1978; Umebayashi & Nakano 1980; Nishi et al. 1991; Sano et al. 2000). For a typical abundance of metal atoms in the gas phase of $8.4 \times 10^{-5}\delta_2$[1] (Umebayashi & Nakano 1990), the radiative recombination rate of metal ions is dominant for all vertical locations of interest, with the exception of the uppermost sections of the disc (see fig. 2 of SW05).

The resulting ionization fraction of the fluid largely determines the ability of the magnetic field to couple to the gas and shear and thus, regulates the magnetic activity in these astrophysical systems. In protoplanetary discs, in particular, the field has been envisioned to be dynamically important near the surface, whereas magnetic activity may be suppressed in their inner sections (the 'layered accretion' scenario; Gammie 1996; Wardle 1997). However, the existence and configuration of a magnetically inactive – dead – zone in the disc interior has been shown to be critically dependent on the presence and properties of dust grains mixed with the gas (W07). As that study shows, in a minimum-mass solar nebula model at 1 au, the entire cross-section of the disc is magnetically coupled when dust grains are assumed to have settled to the mid-plane. It is, in particular, the presence of small grains what most severely affects the magnetic coupling. For example, the presence of a standard interstellar population of 0.1 μm grains at 1 au reduces the total active layer of the disc from ∼1700 to ∼2 g cm$^{-2}$. This column density increases to ∼80 g cm$^{-2}$ once the grains aggregate to 3 μm. At 5 au, in contrast, the entire cross-section of the disc is coupled once the grains have grown to 1 μm (we refer the reader to W07 for further details of these models).

## 3 FORMULATION AND METHODOLOGY

The solutions presented in this paper are based on the formulation detailed in SW05, which is briefly summarized in Appendix A. Essentially, we transform the coordinates $(r, \phi, z, t)$ in the canonical cylindrical frame anchored in the central mass $M$ (e.g. the 'laboratory frame'), to the coordinates $(r, \phi - \Omega t, z, t)$, where $\Omega(r) = \sqrt{GM/r^3}$ is the Keplerian frequency at the radius $r$. In this new frame, therefore, the velocity field is expressed as a *departure* from Keplerian motion $\boldsymbol{v} = \boldsymbol{V} - v_K\hat{\boldsymbol{\phi}}$ (where $\boldsymbol{V}$ is the velocity in the laboratory frame) and $\partial/\partial t + \Omega\partial/\partial\phi$ becomes just $\partial/\partial t$. Note that this is not a 'rotating frame', as $v_K$ retains its radial dependence. This contrasts with the practice to adopt a frame anchored at a fiducial radius $r_0$ [e.g. with $\Omega = \Omega(r_0)$]. In this case, there are extra terms in the governing equations (2) to (4), as we elaborate below.

We further assume that the abundances of charged species are sufficiently low to be able to neglect their inertia, thermal pressure and the effect of ionization and recombination processes on the neutrals. Under these conditions, only the equations of motion for the neutral gas are required:

$$\frac{\partial\rho}{\partial t} + \nabla\cdot(\rho\boldsymbol{v}) = 0, \tag{2}$$

[1] Here, $\delta_2 \approx 0.02$ is the fraction of heavy metal atoms in the gas phase, estimated from interstellar absorption lines in diffuse clouds (Morton 1974).

$$\frac{\partial \boldsymbol{v}}{\partial t} + (\boldsymbol{v}\cdot\nabla)\boldsymbol{v} - 2\Omega v_\phi \hat{\boldsymbol{r}} + \frac{1}{2}\Omega v_{\rm r}\hat{\boldsymbol{\phi}} - \frac{v_{\rm K}^2}{r}\hat{\boldsymbol{r}} + \frac{c_{\rm s}^2}{\rho}\nabla\rho + \nabla\Phi = \frac{\boldsymbol{J}\times\boldsymbol{B}}{c\rho}, \tag{3}$$

$$\frac{\partial \boldsymbol{B}}{\partial t} = \nabla\times(\boldsymbol{v}\times\boldsymbol{B}) - c\nabla\times\boldsymbol{E}' - \frac{3}{2}\Omega \boldsymbol{B}_{\rm r}\hat{\boldsymbol{\phi}}. \tag{4}$$

In the equation of motion (3), $\Phi$ is the gravitational potential for a non-self-gravitating disc and $\boldsymbol{v}_{\rm K}^2/r$ is the centripetal term generated by Keplerian motion. Coriolis terms $2\Omega v_\phi\hat{\boldsymbol{r}}$ and $\frac{1}{2}\Omega v_{\rm r}\hat{\boldsymbol{\phi}}$ are associated with the use of a local Keplerian frame and $c_{\rm s}$ is the isothermal sound speed. In the induction equation (4), $\boldsymbol{E}'$ is the electric field in the frame comoving with the neutrals and $\frac{3}{2}\Omega\boldsymbol{B}_{\rm r}\hat{\boldsymbol{\phi}}$ accounts for the generation of toroidal field by the disc differential rotation. Had we adopted a rotating coordinate system anchored at a fiducial location $r_0$ [e.g. using $\Omega = \Omega(r_0)$], the equation of motion would include an additional term $(r - r_0)\,(\mathrm{d}\Omega/\mathrm{d}R)\,(\partial\boldsymbol{v}/\partial\phi)$ (which is only valid for small radial excursions about $r_0$) and similar terms would also be present in the continuity and induction equations. As discussed above, these terms do not arise in the present formulation because we take $\Omega = \Omega(r)$. Furthermore, for the axisymmetric calculations we present here the extra terms vanish and both formulations are formally identical. Finally, the magnetic field must also satisfy the constraint $\nabla\cdot\boldsymbol{B} = 0$ and the current density must satisfy Ampere's law,

$$\boldsymbol{J} = \frac{c}{4\pi}\nabla\times\boldsymbol{B} \tag{5}$$

and Ohm's law

$$\boldsymbol{J} = \boldsymbol{\sigma}\cdot\boldsymbol{E}'. \tag{6}$$

Following Wardle & Ng (1999) and Wardle (1999; hereafter W99), the current density is expressed as

$$\boldsymbol{J} = \boldsymbol{\sigma}\cdot\boldsymbol{E}' = \sigma_{\rm O}\boldsymbol{E}'_{\parallel} + \sigma_{\rm H}\hat{\boldsymbol{B}}\times\boldsymbol{E}'_{\perp} + \sigma_{\rm P}\boldsymbol{E}'_{\perp}, \tag{7}$$

where subscripts $\parallel$ and $\perp$ denote vector components parallel and perpendicular to $\boldsymbol{B}$. In this expression, $\sigma_{\rm O}$, $\sigma_{\rm H}$ and $\sigma_{\rm P}$ are the Ohmic, Hall and Pedersen conductivity terms given by

$$\sigma_{\rm O} = \frac{ec}{B}\sum_j n_j Z_j \beta_j, \tag{8}$$

$$\sigma_{\rm H} = \frac{ec}{B}\sum_j \frac{n_j Z_j}{1+\beta_j^2} \tag{9}$$

and

$$\sigma_{\rm P} = \frac{ec}{B}\sum_j \frac{n_j Z_j \beta_j}{1+\beta_j^2}. \tag{10}$$

The subscript $j$ is used here to label the charged species. They are characterized by their number density $n_j$, particle mass $m_j$, charge $Z_j e$ and Hall parameter

$$\beta_j = \frac{Z_j e B}{m_j c}\frac{1}{\gamma_j\rho} \tag{11}$$

(the ratio of the gyrofrequency and the collision frequency with the neutrals), which measures the relative importance of the Lorentz and drag forces in balancing the electric force on the particle.

Equation (7) can be inverted to find an expression for $\boldsymbol{E}'$. This leads to the following form of the induction equation (W07)

$$\frac{\partial \boldsymbol{B}}{\partial t} = \nabla\times(\boldsymbol{v}\times\boldsymbol{B}) - \nabla\times[\eta_{\rm O}\nabla\times\boldsymbol{B} + \eta_{\rm H}(\nabla\times\boldsymbol{B})\times\hat{\boldsymbol{B}} + \eta_{\rm A}(\nabla\times\boldsymbol{B})_\perp], \tag{12}$$

where

$$\eta_{\rm O} = \frac{c^2}{4\pi\sigma_{\rm O}}, \tag{13}$$

$$\eta_{\rm H} = \frac{c^2}{4\pi\sigma_\perp}\frac{\sigma_{\rm H}}{\sigma_\perp} \tag{14}$$

and

$$\eta_{\rm A} = \frac{c^2}{4\pi\sigma_\perp}\frac{\sigma_{\rm P}}{\sigma_\perp} - \eta_{\rm O} \tag{15}$$

are the Ohmic, Hall and ambipolar diffusivities; and

$$\sigma_\perp = \sqrt{\sigma_{\rm H}^2 + \sigma_{\rm P}^2} \tag{16}$$

is the total conductivity perpendicular to the magnetic field. When ions and electrons are the only charged species, it can be shown that (W07)

$$|\eta_{\rm H}| = |\beta_{\rm e}|\eta_{\rm O} \tag{17}$$

and

$$\eta_{\rm A} = |\beta_{\rm e}|\beta_{\rm i}\eta_{\rm O}. \tag{18}$$

Note that the Ohmic ($\eta_{\rm O}$) and ambipolar ($\eta_{\rm A}$) diffusivity terms are always positive, as the former does not depend on the magnetic field strength and the second scale quadratically with it. As a result, they are both invariant under a reversal of the magnetic field polarity. On the contrary, the Hall term ($\eta_{\rm H}$) scales linearly with $B$ and thus, can become negative. The change in sign of $\eta_{\rm H}$ corresponds, in turn, to a change in the direction of the magnetic field at the height where particular species become decoupled to it by collisions with the neutrals. It corresponds, therefore, to changes in the contribution of different charged species to this component of the diffusivity tensor.

The relative importance of the diffusion terms in (13) to (15) differentiates three *diffusivity regimes*.

(i) In the *Ambipolar diffusion* regime, $|\beta_j| \gg 1$ for most charged species and $\eta_{\rm A} \gg |\eta_{\rm H}| \gg \eta_{\rm O}$. In this limit, which is typically dominant in low-density regions (e.g. in molecular clouds and near the surface of protoplanetary discs), the magnetic field is effectively frozen into the ionized component of the fluid and drifts with it through the neutrals.

(ii) *Ohmic* (*resistive*) *limit*. In this case, $|\beta_j| \ll 1$ for most charged species, resulting in $\eta_{\rm O} \gg |\eta_{\rm H}| \gg \eta_{\rm A}$. The magnetic field cannot be regarded as being frozen into any fluid component and the diffusivity is a scalar, the well-known Ohmic diffusivity. This regime dominates close to the mid-plane in the inner regions ($R \lesssim 5$ au) of protoplanetary discs when the magnetic field is relatively weak (W07).

(iii) *Hall diffusion* limit, which occurs when $|\beta_j| \gg 1$ for charged species of one sign (typically electrons) and $\ll 1$ for those of the other sign (e.g. ions). In this case, $|\eta_{\rm H}| \gg \eta_{\rm A}$ and $\eta_{\rm O}$. This regime is important at intermediate densities (between those at which ambipolar and Ohmic diffusion regimes dominate). It has been shown to prevail under fluid conditions satisfied over vast regions in protoplanetary discs (e.g. Sano & Stone 2002a, W07).

The diffusivities used in this study were calculated using the procedure described in W07, to which we refer the reader for details. Essentially, the adopted chemical reaction scheme is based on that of Nishi et al. (1991), but it allows for higher charge states on dust grains. This is necessary because of the higher temperature and density of protoplanetary discs in relation to those typically associated with molecular clouds.

Finally, in the following sections, we will also use the magnetic coupling parameter (W99)

$$\chi \equiv \frac{\omega_c}{\Omega} = \frac{1}{\Omega}\frac{B^2\sigma_\perp}{\rho c^2}, \tag{19}$$

the ratio of the critical frequency ($\omega_c$) *above* which flux-freezing conditions break down and the dynamical (Keplerian) frequency of the disc. For the sake of clarity, we now sketch the arguments leading to this expression (see also Wardle & Ng 1999). First, recall that non-ideal-MHD effects become important when the inductive and diffusive terms in the induction equation (4) are comparable; or

$$\nabla \times (\boldsymbol{v} \times \boldsymbol{B}) \sim c\nabla \times \boldsymbol{E}', \tag{20}$$

where (see equation 6)

$$\boldsymbol{E}' = \frac{\boldsymbol{J}}{\sigma} = \frac{1}{\sigma}\left(\frac{c}{4\pi}\nabla \times \boldsymbol{B}\right). \tag{21}$$

In expression (21), $\sigma$ is taken to be a characteristic measure of the conductivity of the gas. Next, we adopt the following typical values for the various terms above

$$\nabla \sim k = \omega/v_A \qquad v \sim v_A \qquad B \sim B_0 \qquad \sigma \sim \sigma_\perp,$$

where $k$ is the wavenumber of the MRI perturbations in flux-freezing conditions and $v_A \equiv B^2/4\pi\rho$ is the local Alfvén speed. Substituting these relations in (20) yields the desired expression for $\omega_c$. This parameter is useful because in ideal-MHD conditions, the instability grows at $\sim$0.75$\Omega$ (Balbus & Hawley 1991). Consequently, if $\omega_c < \Omega$ (or $\chi < 1$) the field is poorly coupled to the disc at the frequencies of interest for the analysis of the MRI and non-ideal-MHD effects are expected to be important.

Equations (2)–(5) and (7) are linearized about an initial (labelled by a subscript 'I'), steady state where the magnetic field is vertical and the current density, fluid velocity and electric field in the frame comoving with the neutrals all vanish. As a result of the last condition, the changes in the components of the diffusivity tensor are not relevant in this linear formulation (e.g. $\boldsymbol{E}'_I \cdot \delta\boldsymbol{\sigma} \equiv 0$) and only the initial, unperturbed values are required. Taking perturbations of the form $\boldsymbol{q} = \boldsymbol{q}_I + \delta\boldsymbol{q}(z)e^{i\omega t}$, we obtain a system of ordinary differential equations (ODE) in $\boldsymbol{\delta E}$ (the perturbations of the electric field in the laboratory frame), $\boldsymbol{\delta B}$ and the perturbations' growth rate $\nu = i\omega/\Omega$. The above procedure is detailed in SW03. Specifically, the linearization of the equations is developed in Section 3.1 of that paper, and the system of ODEs is given in their equations (54)–(57). For the sake of clarity, the final, linearized, equations are reproduced in Appendix A.

Three parameters are found to control the dynamics and evolution of the fluid: (i) $v_A/c_s$, the local ratio of the Alfvén speed and the isothermal sound speed of the gas, which measures the strength of the magnetic field. (ii) $\chi$, the coupling between the ionized and neutral components of the fluid. (iii) $\eta_H/\eta_P$, the ratio of the diffusivity terms perpendicular to $\boldsymbol{B}$, which characterizes the diffusivity regime of the fluid. These parameters are evaluated at different locations $(r, z)$ of the disc taking the magnetic field strength ($B >$ 1 mG) as a free parameter. The system of equations is integrated vertically as a two-point boundary value problem for coupled ODE with boundary conditions $\delta B_r = \delta B_\phi = 0$ and $\delta E_r = 1$ at $z = 0$ and $\delta B_r = \delta B_\phi = 0$ at $z/H = 6$. As discussed in SW03, these boundary conditions are strictly valid at infinity, but can also be applied at a boundary located sufficiently high above the mid-plane. This particular height was chosen after confirming that increasing the location of the boundary does not significantly affect either the structure or the growth rate of the MRI-unstable modes.

Given that magnetic diffusion can have such a dramatic effect on the properties of magnetically driven turbulence in protoplanetary discs, we now present calculations of the magnetic diffusivity at 5 and 10 au. We explore which disc regions are expected to be magnetically coupled and which diffusion mechanism is dominant at different positions $(r, z)$ as a function of $B$. This discussion is relevant for the analysis of our MRI results at these locations (Section 4).

### 3.1 Magnetic diffusivity

Fig. 1 shows the components of the diffusivity tensor ($\eta_O$, $|\eta_H|$ and $\eta_A$) as a function of height for $R = 10$ au and a representative field strength ($B = 10$ mG). The solutions in the top panel have been obtained assuming that dust grains have settled into a thin layer about the mid-plane, so the charges are carried by ions and electrons only. The results in the middle and bottom panels incorporate a population of 1 and 0.1 μm-sized grains, respectively. Note that when dust grains are present, all diffusivity terms increase drastically in relation to their values in the no-grains scenario. This effect becomes more accentuated as the grain size diminishes, given the efficiency of small grains in removing free electrons from the gas. For example, in the case that incorporates 0.1 μm-sized particles (bottom panel), the diffusivity components at the mid-plane are larger, by 4–7 orders of magnitude, than their corresponding values when the grains have settled.

When dust grains have either settled or aggregated to at least 1 μm in size (see top and middle panels), $|\eta_H|$ is dominant for $z/H \lesssim 2.5$ and the fluid in this region is in the Hall diffusivity regime. Also, $\eta_A > \eta_O$ there which implies that, if ions and electrons are the sole charge carriers, $|\beta_e|\,\beta_i > 1$ (see equation 18). For higher $z$, $\eta_A > |\eta_H| > \eta_O$ and ambipolar diffusion dominates. Note that the Hall diffusivity term increases less sharply than the ambipolar diffusivity in response to the fall in fluid density. This is a general feature, and an expected one, given that the former scales with $\rho^{-1}$ and the latter with $\rho^{-2}$. As a result, $\eta_A$ is typically several orders of magnitude larger than $|\eta_H|$ near the surface regions of the disc. Finally, for the 0.1 μm-sized grain population (bottom panel), $\eta_A > |\eta_H|$ for all $z$. This can be traced back to the fact that Hall diffusion is suppressed here because of the nearly equal abundances of (negatively charged) grains and ions in this region.

Note also that the Hall diffusivity component shows characteristic 'spikes', at the heights where it changes sign. This effect is also particularly evident for the 0.1 μm-sized grains. In this scenario, in particular, $\eta_H$ is positive when $0 \lesssim z/H \lesssim 1.6$ and $2.5 \lesssim z/H \lesssim 4.1$. It is negative at all other vertical locations. As mentioned above, this corresponds to different charged species contributing to this diffusion term. In order to explore the contributions to $\eta_H$ in each of the vertical sections in which it has a different sign, we now describe the behaviour of the charged species at four representative heights, namely $z/H = 1$ and 3 (for which $\eta_H > 0$), and $z/H = 2$ and 5 (where $\eta_H < 0$).

At $z/H = 1$, the density is sufficiently high for electrons to be able to stick to the grains. As a result, they reside mainly on dust particles, as do about a third of the ions. The contribution of (negatively charged) grains and ions to the Hall diffusivity term is very similar, with a small positive excess, which determines the sign of $\eta_H$ in this region. On the contrary, at $z/H = 2$, ions are the dominant positively charged species, while the negative charges are still contained in dust grains and drift together with the neutrals. Consequently, $\eta_H$ is negative in this section of the disc. At $z/H = 3$,

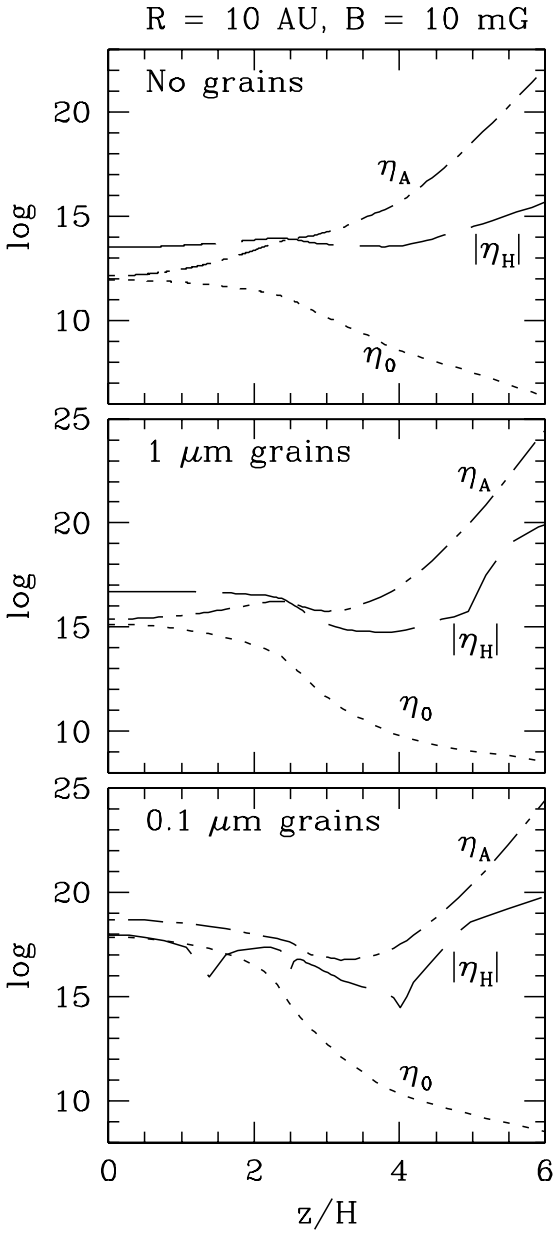


**Figure 1.** Components of the diffusivity tensor ($\eta_O$,$|\eta_H|$ and $\eta_A$) as a function of height for $R = 10$ au and $B = 10$ mG (corresponding to a mid-plane ratio of the Alfvén to sound speed $v_{A0}/c_s = 0.03$). In the top panel, dust grains have settled to the mid-plane. The middle and bottom panels show the solutions when dust grains of radius $a = 1$ and 0.1 μm, respectively, are well mixed with the gas over the entire disc thickness. When the grains are $\gtrsim$1 μm in size (or are absent), Hall diffusion dominates for $z/H \lesssim 2.5$. In contrast, for the 0.1 μm-sized grains, $\eta_A > |\eta_H|$ for all $z$ and $|\eta_H| > \eta_O$ above $z/H \sim 1$. Note that $|\eta_H|$ shows 'spikes' at the $z$ where it changes sign in response to different charged species becoming decoupled to the magnetic field by collisions with the neutrals.

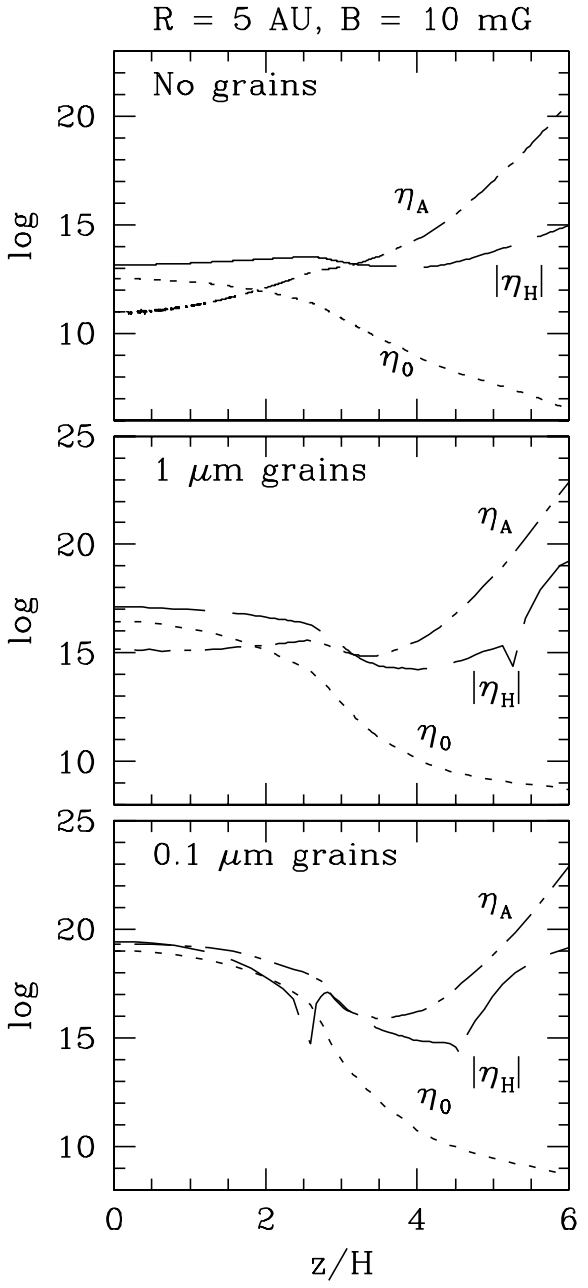


**Figure 2.** As per Fig. 1 for $R = 5$ au and $B = 10$ mG ($v_{A0}/c_s = 0.01$). Note that when the grains are $\gtrsim$1 μm in size or are absent (top and middle panels), Hall diffusion dominates for $z/H \lesssim 3$. At this radius, however, $\eta_O > \eta_A$ for $z/H \lesssim 2$.

ions and electrons are the main charge carriers and ions dominate the contribution to the Hall term, which makes $\eta_H$ positive. Finally, for $z/H = 5$, the dominant contribution to the Hall diffusivity term comes from the small percentage of remaining negatively charged grains. As a result, $\eta_H$ is negative (and very small).

We now turn our attention to $R = 5$ au (Fig. 2). At this radius, when the dust particles are at least 1 μm in size (or are absent), Hall diffusion dominates for $z/H \lesssim 3$. In contrast with the solutions at 10 au, however, Ohmic diffusion dominates over ambipolar diffusion ($\eta_O > \eta_A$) for most of this region (which implies that $|\beta_e|\beta_i < 1$ in this section of the disc when no grains are present). This is expected, given the larger fluid density at this radius in comparison with the 10 au case discussed above. When the grains are small ($a = 0.1$ μm, see bottom panel), ambipolar diffusion is dominant ($\eta_A > |\eta_H| > \eta_O$) for $1 \lesssim z/H \lesssim 2.8$ and $z/H \gtrsim 3.5$. At all other heights, $\eta_A \approx |\eta_H| > \eta_O$.

Figs 3 and 4 generalize the analysis of the previous paragraphs to other field strengths for $R = 10$ and 5 au, respectively. As before, the top panels refer to discs where no grains are present. The middle and bottom panels incorporate 1 and 0.1 μm-sized grains, respectively.

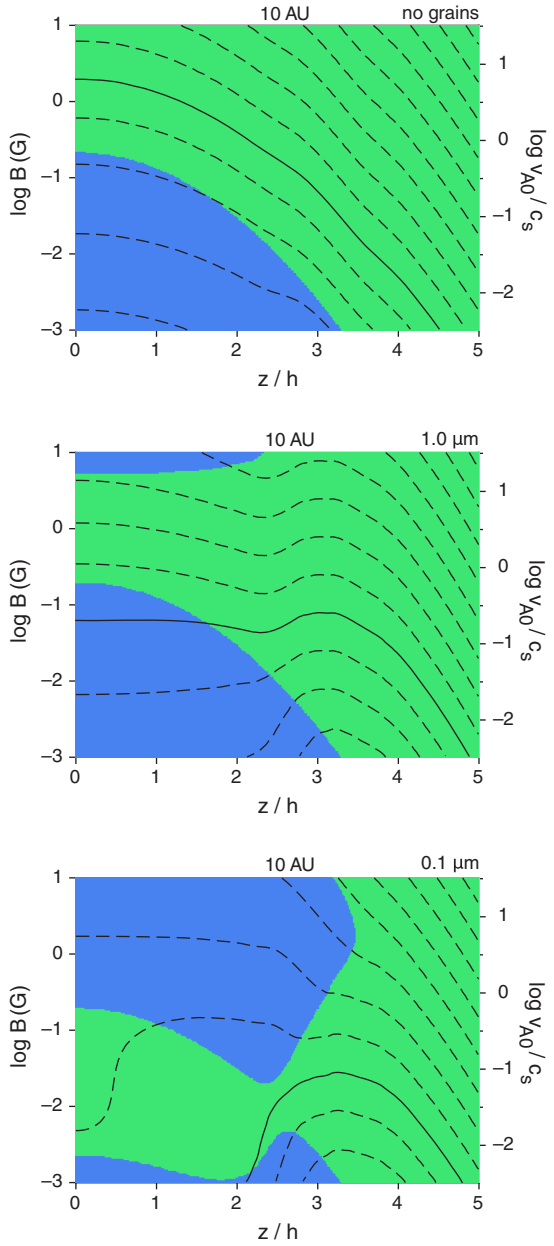


**Figure 3.** Contours of $\tilde{\eta} \equiv (\eta_{\rm O}^2 + \eta_{\rm H}^2 + \eta_{\rm A}^2)^{1/2}$ in a log($B$)–$z/H$ plane for $R = 10$ au. In the top panel, dust particles are assumed to have settled to the mid-plane. The effect of dust grains is included in the middle ($a =$ 1 μm) and bottom ($a = 0.1$ μm) panels. The solid line is the critical value of the diffusivity $\tilde{\eta}_{\rm crit} \equiv Hc_{\rm s}$ (W07) above which the magnetic field does not couple to the gas and shear. The background shading (from dark to light) denotes the dominant diffusion mechanism as Ohmic, Hall or Ambipolar. Note that when the grain size is 1 μm or larger (or they have settled), the disc mid-plane is magnetically coupled for a range of $B$. In contrast, when the grains are small (bottom panel), magnetic diffusion prevents the field to couple to the gas for $z/H \lesssim 2$.

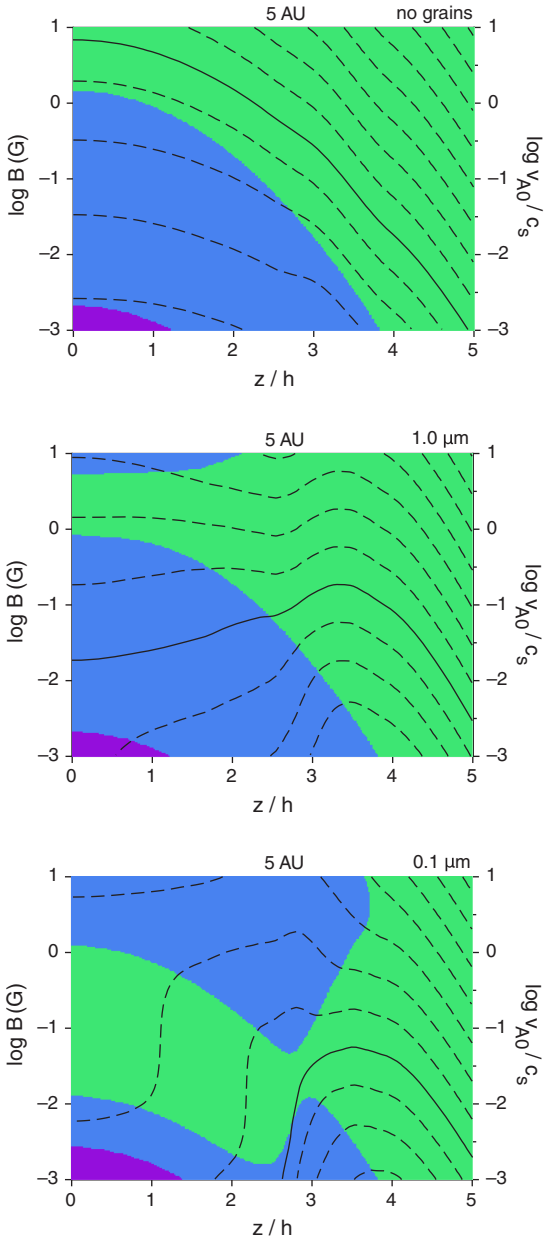


**Figure 4.** As per Fig. 3 for $R = 5$ au. Note that in all cases, Ohmic diffusion is dominant close to the mid-plane ($z/H \lesssim 1.2$) when the field is weak ($B <$ a few mG). The mid-plane can be magnetically coupled when the grains are absent or have aggregated to $a \gtrsim 1$ μm. However, a dead zone develops below ∼2.5 scaleheights when they are small ($a = 0.1$ μm). In this scenario, only $B \lesssim 50$ mG can couple to the gas (and only for $z/H \gtrsim 2.5$). Note that ambipolar diffusion dominates for all $B$ when $z/H \gtrsim 4$ (all panels) and for 1 mG $\lesssim B \lesssim$ 10–100 mG below this height (bottom panel only).

In these plots, the contours show the values of $\tilde{\eta} \equiv (\eta_{\rm O}^2 + \eta_{\rm H}^2 + \eta_{\rm A}^2)^{1/2}$ and the background shading (from dark to light) denotes the dominant diffusion mechanism as Ohmic, Hall or Ambipolar. The solid line is the critical value of the diffusivity $\tilde{\eta}_{\rm crit} \equiv Hc_{\rm s}$ (W07), above which the diffusion term in the induction equation $|\nabla \times (\tilde{\eta} \nabla \times \boldsymbol{B})|$ is larger than the inductive term $|\nabla \times (\boldsymbol{v} \times \boldsymbol{B})|$ (see equation 4), a situation that effectively limits the ability of the field to couple to the Keplerian shear. The dashed lines correspond to increase (decrease) in $\tilde{\eta}$ by the factors of 10 in the direction of a stronger (weaker) magnetic field.

Note that at 10 au, in the no-grains case (top panel of Fig. 3), field strengths $\lesssim$ a few Gauss are able to couple to the gas at the mid-plane. Hall diffusion dominates at this location for $B \lesssim 0.1$ G but the range of field strengths over which this occurs decreases gradually with height, so that when $z/H \gtrsim 3.3$ ambipolar diffusion

is dominant for all $B$. The coupled region potentially extends to $z/H \sim 4.5$, depending on the field strength. When the particles have aggregated to 1 μm in size (middle panel of Fig. 3), the situation is qualitatively similar to the one just discussed, the only significant difference being that in this case Hall diffusion is dominant at the mid-plane for all $B$ that can couple to the gas.

The previous results, however, are significantly modified when small dust grains are present ($a = 0.1$ μm, bottom panel). In this case, the section of the disc below two scaleheights is magnetically inactive and the magnetic diffusivity is severe enough to prevent coupling over the entire disc thickness when $B \gtrsim 25$ mG. Ambipolar diffusion dominates for all field strengths above approximately four scaleheights and also for $\sim 1 \lesssim B \lesssim$ 10–100 mG below this height (the actual upper limit of this range varies with $z$). Hall diffusion is inhibited close to the mid-plane for this range of field strengths because the number density of positively and negatively charged grains is very similar. Note, finally, that Ohmic diffusion is not dominant in any of the depicted scenarios at this radius, as expected, given the relatively low density of the fluid.

The results at 5 au are qualitatively similar (Fig. 4) to the ones just discussed. One key difference, however, is that Ohmic diffusion dominates in all cases for $z/H \lesssim 1.2$ provided that the field is sufficiently weak ($B \lesssim$ a few milligauss). Ambipolar diffusion, on the other hand, is dominant for relatively strong fields (e.g. $B \gtrsim 1$ G at $z = 0$ in the no-grains case) as well as for all $B$ near the disc surface ($z/H \gtrsim 4$). Hall diffusivity is the most important diffusion mechanism for fluid conditions in-between those specified above. Note that the coupled region extends up to $z/H \sim 5$ in all cases. When no grains are present (top panel), the mid-plane is coupled for fields up to a few Gauss. This upper limit drops to ∼20 mG when 1 μm grains are mixed with the gas. When the grains are 0.1 μm in size, however, only the region above $z/H \sim 2.5$ is coupled, and only for $B \lesssim 50$ mG. This 'dead' zone is slightly more extended at this radius than at 10 au, but stronger fields are able to couple to the gas in this case. The steep contours close to the mid-plane in this scenario result from the pronounced increase in the diffusivity in response to the increase in fluid density and the decline in the ionization fraction of the gas as $z$ diminishes.

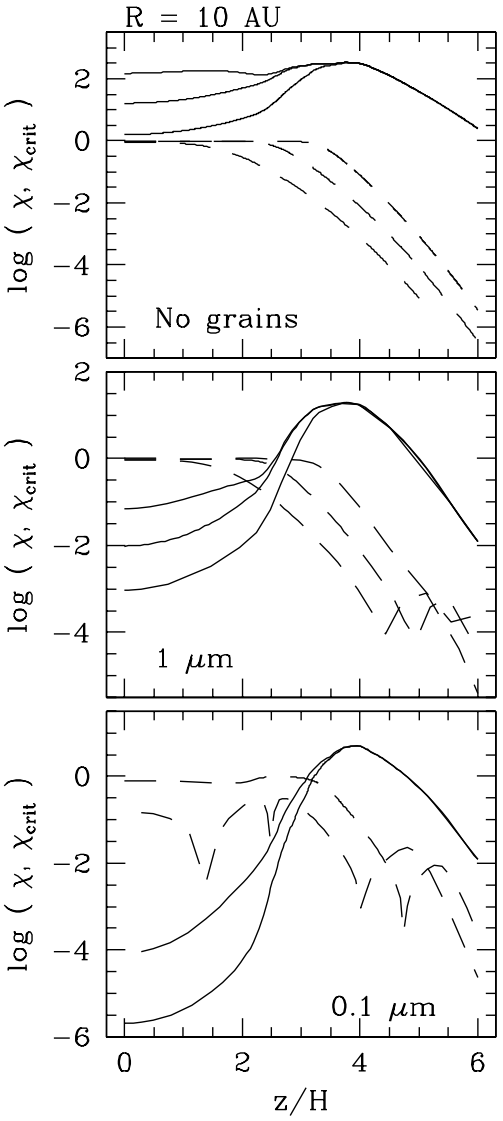


**Figure 5.** Comparison of the local magnetic coupling $\chi$ (solid lines) and critical coupling $\chi_{\rm crit} \equiv |\sigma_{\rm H}|/\sigma_\perp$ (dashed lines) for $R = 10$ au as a function of the magnetic field strength and for different assumptions regarding the presence (and size) of dust grains. Hall diffusion modifies the structure and growth rate of MRI-unstable modes in the regions where $\chi < \chi_{\rm crit}$ provided that the coupling is sufficient for the instability to operate (SW03). Ambipolar diffusion is important if $\chi_{\rm crit} < \chi \lesssim 10$. For stronger $\chi$, ideal-MHD describes the fluid adequately (W99). The bottom (and leftmost) lines correspond to $B = 1$ mG ($v_{\rm A0}/c_{\rm s} = 0.003$) in all panels. $B$ and $v_{\rm A0}/c_{\rm s}$ increase by a factor of 10 between curves (towards larger $\chi$), except that the top curve for $a = 1$ μm grains corresponds to $B = 77$ mG ($v_{\rm A0}/c_{\rm s} = 0.25$), the strongest field for which perturbations grow.

### 3.2 Magnetic coupling and MRI-unstable modes

In this section, we address the following question: which magnetic diffusion mechanism determines the properties of the MRI in different regions in protoplanetary discs? In this connection, it is useful to recall (see W99, SW03 and references therein for details) that in the disc regions where the magnetic coupling $\chi > 10$, ideal-MHD conditions hold and the particular configuration of the diffusivity tensor has little effect on the behaviour of the MRI. When $\chi$ is weaker than this but $\gtrsim |\sigma_{\rm H}|/\sigma_\perp$, ambipolar diffusion dominates. Finally, in the regions where $\chi < |\sigma_{\rm H}|/\sigma_\perp$, Hall diffusion modifies the structure and growth of MRI-unstable modes, provided that this degree of coupling is sufficient for unstable modes to grow.

Figs 5 and 6 compare $\chi$ with the ratio $|\sigma_{\rm H}|/\sigma_\perp$ at $R = 10$ and 5 au, respectively, as a function of the magnetic field strength and for different assumptions regarding the presence, and radius, of dust grains mixed with the gas. In each figure, the top panels depict the results obtained assuming that no grains are present whereas the effect of 1 μm (0.1 μm)-sized grains is shown in the middle (bottom) panels. Note the dramatic impact dust grains have in the level of magnetic coupling at both radii. For example, introducing a population of 0.1 μm grains causes $\chi$ to drop by 6–8 orders of magnitude at the mid-plane. Bottom (solid) and leftmost (dashed) lines correspond to $B = 1$ mG in all the cases. The field strength increases by a factor of 10 towards larger $\chi$, except that at both radii the top (and rightmost) curves for $a = 1$ μm show the maximum field strength for which the MRI grows. This is also the case for the solutions with no grains at 5 au (the maximum values of $B$ for these cases are noted in the captions of Figs 5 and 6).

Note that at 10 au (Fig. 5), Hall diffusion is not expected to play an important role in the local properties of the MRI once the grains have settled ($\chi > |\sigma_{\rm H}|/\sigma_\perp$ for all $z$ and $B$). In this scenario, ambipolar diffusion dominates in the inner sections of the disc when

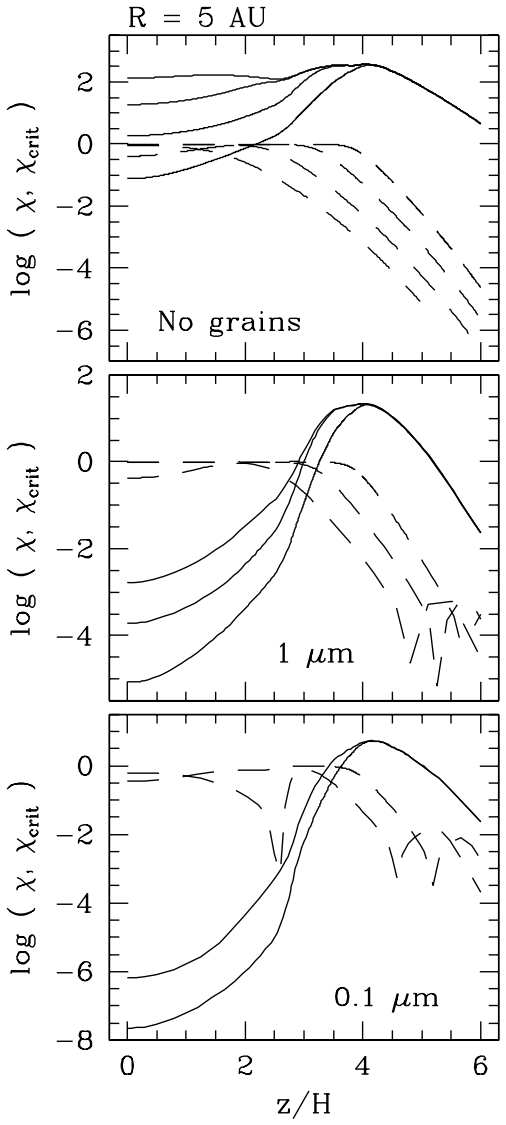


**Figure 6.** As per Fig. 5 for $R = 5$ au. The bottom (and leftmost) lines also correspond to $B = 1$ mG ($v_{A0}/c_s = 0.001$). Note, however, that the top (and rightmost) lines in the top panel correspond to $B = 795$ mG ($v_{A0}/c_s = 0.83$) and to $B = 83$ mG ($v_{A0}/c_s = 0.09$) in the middle panel. They are the maximum field strengths for which unstable modes grow in those scenarios.

the field is weak ($z/H \lesssim 2$ and $B \lesssim 10$ mG) while ideal-MHD holds at all heights for stronger $B$. On the contrary, when either 1 μm or 0.1 μm-sized grains are mixed with the gas (middle and bottom panels), Hall diffusion has an impact on the MRI within approximately three scaleheights of the mid-plane. At higher $z$, the ionization fraction is such that $|\sigma_H|/\sigma_\perp \lesssim \chi \lesssim 10$ and ambipolar diffusion determines the local properties of MRI-unstable modes.

The corresponding solutions at 5 au are shown in Fig. 6. In this case, Hall diffusion dominates within two scaleheights from the mid-plane if the magnetic field is weak ($B \lesssim 10$ mG) and the grains have settled (top panel). This is consistent with the higher column density at this radius in comparison to the 10 au case discussed above (for which Hall diffusion was unimportant). Ambipolar diffusion is dominant in this scenario for 10 mG $\lesssim B \lesssim$ 100 mG but for stronger fields, $\chi > 10$ for all $z$ and the fluid is in ideal-MHD conditions over the entire section of the disc. On the other hand, when dust grains are present (middle and bottom panels), Hall diffusion determines the properties of MRI-unstable modes in the inner sections of the disc ($z/H \lesssim 3$) for all magnetic field strengths for which they grow. Ambipolar diffusion is locally dominant at higher $z$.

Finally, note that when dust grains are present, the extent of the disc section where Hall diffusion has an impact on the MRI at both radii is quite insensitive to the strength of the field. Evidently, dust particles can efficiently reduce the degree of magnetic coupling in the disc inner sections for a wide range of magnetic field strengths. In light of the concepts presented so far, we now analyse the properties of the MRI at the two radii of interest.

## 4 MAGNETOROTATIONAL INSTABILITY

Figs 7 and 8 compare the vertical structure and growth rate of the most unstable MRI modes at $R = 10$ and 5 au, respectively, for different choices of the magnetic field strength. The left-hand side column of each figure displays solutions obtained assuming that grains have settled out of the gas phase. The remaining columns – from left- to right-hand side – show results that incorporate the effect of a different population of single-sized dust particles of radius $a = 3$, 1 and 0.1 μm, respectively. Note how the growth rate, wavenumber and range of magnetic field strengths for which unstable modes exist are all drastically diminished when dust grains are present. This is expected, given the reduction in the coupling between the neutral and ionized components of the fluid when dust grains (particularly if they are small) are well mixed with the gas. Note also that the range of field strengths for which unstable modes are found matches quite well with the range for which the magnetic field is expected to couple to the fluid, as discussed in Section 3.1 (see Figs 3 and 4 and compare the maximum magnetic field strength for which the MRI grows and the maximum $B$ that can couple to the gas at the $z$ where the modes peak).

For the discussion that follows, it is useful to keep in mind that both the growth rate and the envelope of these perturbations are shaped by the interplay of different diffusion mechanisms, whose relative importance vary strongly with height. In particular, the ambipolar diffusion component of the diffusivity tensor drives the local growth rate (and thus the amplitude of global perturbations) to increase with $z$ (SW03). This is because, in this diffusion regime, the maximum growth rate increases with the local $\chi$ (W99) and is, therefore, a strong function of the vertical location. Accordingly, the envelopes of the perturbations driven by this term typically peak at an intermediate height above the mid-plane. On the contrary, the maximum growth rate of Hall perturbations is insensitive to $\chi$ (W99). Because they are not driven from any particular vertical location, their envelope is fairly flat (SW03). We now analyse the structure and growth of the perturbations at the two radii of interest. The properties of these modes without dust grains were discussed in detail in SW05. For the sake of clarity, these results are briefly summarized as part of this discussion.

At 10 au, ambipolar diffusion drives the MRI when the field is weak ($B \lesssim 10$ mG) and ions and electrons are the sole charge carriers (see top panel of Fig. 5). As a result, unstable modes peak above the mid-plane in this scenario (left-hand side column of Fig. 7; e.g. the mode computed with $B = 1$ mG peaks at $z/H \sim 0.5$). For stronger fields, ideal-MHD holds at all $z$. This explains the flat envelope, and fast growth, of the perturbations obtained with $B = 10$ and 100 mG. Unstable modes are found in this case for $B \lesssim 250$ mG and they grow at about the ideal-MHD rate for $2 \lesssim B \lesssim 50$ mG. When $B$ is even stronger than 250 mG, the wavelength of the most unstable mode is $\sim H$, the disc tidal scaleheight and the

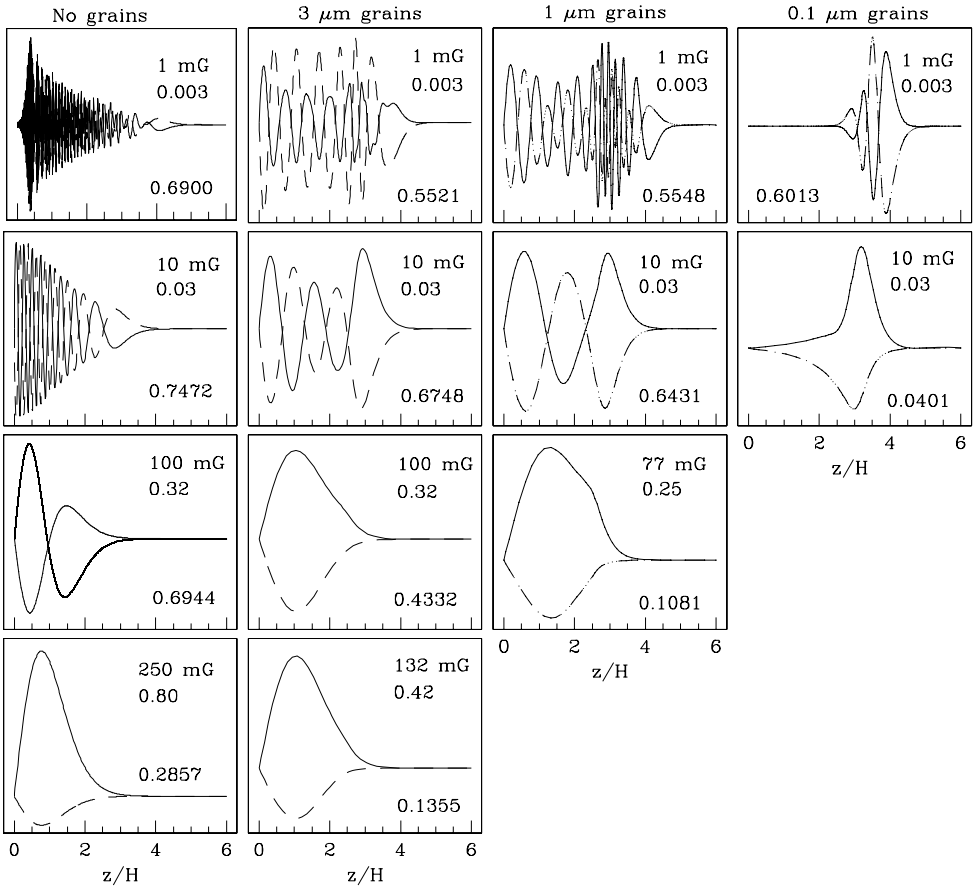


**Figure 7.** Structure and growth rate of the fastest growing MRI modes for $R = 10$ au and different choices of the magnetic field strength. The leftmost column shows the perturbations obtained if dust grains have settled, while the remaining ones, from left- to right-hand side, display results assuming a population of single-sized grains of radius $a = 3$, 1 and 0.1 μm, respectively, are well mixed with the gas. The growth rate is indicated in the lower portion of each panel. The strength of the field and the mid-plane ratio of the Alfvén to sound speed ($v_{A0}/c_s$) appear at the top. Results are displayed for $B$ spanning from 1 mG, the weakest magnetic field for which unstable modes could be computed, to the maximum strength for which unstable modes were found in each case. Note the reduced wavenumber, growth rate and range of $B$ for which perturbations exist – as well as the extended dead zone – when dust grains are present. When the grains are relatively large (central two columns), Hall diffusion controls the modes, which grow even at the mid-plane. In contrast, when they are small (right-hand side column), the magnetic coupling is too low to sustain the instability for $z/H \lesssim 3$ and ambipolar diffusion controls the perturbations that grow above this height.

perturbations are strongly damped (Balbus & Hawley 1991). Finally, note that no dead zone develops in this scenario, given that the magnetic field is coupled to the gas even at the mid-plane (see top panel of Fig. 3).

We now turn our attention to the solutions obtained under the assumption that dust grains are present at this radius. Note that when the dust particles are relatively large ($a = 3$ and 1 μm, central two columns of Fig. 7), the perturbations exhibit the flat envelope that is typical when Hall diffusion controls their behaviour (for these fluid conditions Hall diffusion is expected to modify MRI modes for $z/H \lesssim 2.5$, Fig. 5). These modes grow even at the mid-plane, a result consistent with the level of magnetic coupling associated with this disc model (e.g. see middle panel of Fig. 3). On the other hand, when the dust grains are small (rightmost column of Fig. 7), the low-magnetic coupling, especially within two scaleheights of the mid-plane (Fig. 3, bottom panel), causes the amplitude of all perturbations in this section of the disc to be severely reduced. Unstable modes were found here only for $B \lesssim 10$ mG, a much reduced range compared with the $B \approx 250$ mG for which they exist when ions and electrons are the only charge carriers.

Fig. 8 shows the solutions obtained for $R = 5$ au. At this radius, MRI-unstable modes grow – without grains – for $B \lesssim 795$ mG. Moreover, they grow at essentially the ideal-MHD rate for a significant subset of this range ($200 \lesssim B \lesssim 500$ mG). Hall diffusion modifies the structure and growth of these modes for $B \lesssim 10$ mG. When the field is within this limit, a small magnetically dead region develops but it disappears for stronger $B$. Note that all the solutions that incorporate dust grains peak at a height above the mid-plane where ambipolar diffusion is locally dominant (e.g. $z/H \sim 4$ for $B = 10$ mG and $a = 1$ μm; see also the middle panel of Fig. 6). This signals that this diffusivity term shapes the structure of these perturbations and explains why their amplitude increases with height. The solutions computed with the small grain population ($a = 0.1$ μm) exhibit, as in the $R = 10$ au case, an extended dead zone encompassing the region where the magnetic coupling is insufficient to sustain the MRI ($z/H \lesssim 2.5$; see bottom panel of Fig. 4). Solutions are found in this case for $B \lesssim 16$ mG.

The solutions described so far in this section incorporate all diffusion mechanisms (represented by $\eta_A$, $\eta_H$ and $\eta_O$). For comparison, Fig. 9 displays how the full $\boldsymbol{\eta}$ modes at 10 au and including 0.1 μm-sized grains (left-hand side column), are modified if only ambipolar

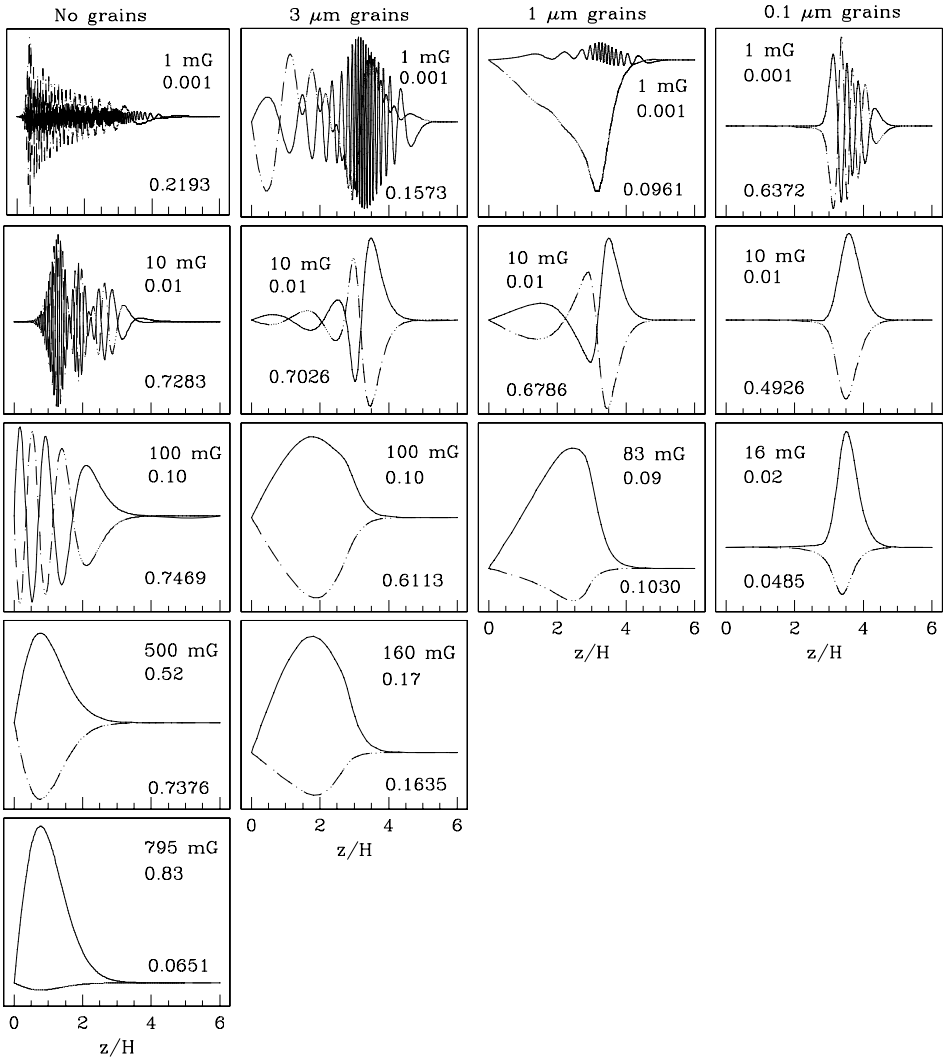


**Figure 8.** As per Fig. 7 for $R = 5$ au. At this radius, the solutions that incorporate 3 and 1 μm-sized grains (central two columns) are shaped by ambipolar diffusion, as this mechanism is dominant at the height where they peak (see middle panel of Fig. 6). Note the extended dead zone when the grains are small (right-hand side column). In this scenario, severe magnetic diffusivity prevents the magnetic field from coupling to the gas for $z/H \lesssim 2.5$ and ambipolar diffusion dominates at higher $z$ where the MRI grows.

diffusion (middle column) and Hall diffusion (right-hand side column) are considered. Note that when the field is weak (e.g. the solutions for $B = 1$ and 4 mG), full $\boldsymbol{\eta}$ perturbations grow faster, and are active closer to the mid-plane, than modes obtained in the ambipolar diffusion limit. This is the result of the contribution of the Hall diffusivity term (e.g. note that the solution in the Hall limit for $B = 1$ mG grows at the ideal-MHD rate). For $B = 10$ mG, the structure of the modes computed with and without the Hall term is fairly similar, as this diffusion mechanism is no longer important at the $z$ where they peak (see bottom panel of Fig. 3). Note also that modes in the Hall limit do not grow for $B > 4$ mG, a result consistent with ambipolar diffusion being dominant at these field strengths (see bottom panel of Fig. 3).

A similar comparison is shown in Fig. 10 for $R = 5$ au and incorporating the effect of 3 μm-sized dust particles. The Hall term is important here also, as evidenced by the faster growth and more extended unstable zone of the perturbations that include this diffusion mechanism. Ambipolar diffusion strongly influences the structure of the modes for intermediate field strengths (e.g. compare the solutions with $B = 10$ mG and different configurations of the diffusivity tensor) and the perturbations grow in this limit for a reduced range of $B$ in relation to that associated with full $\boldsymbol{\eta}$ (or Hall limit) modes.

The dependence of the growth rate of the most unstable mode ($\nu_{\max}$) with the strength of the magnetic field is summarized in Fig. 11 for different assumptions regarding the presence, and radius, of dust grains mixed with the gas. Results are shown for $R = 10$ au (left-hand panel) and 5 au (right-hand panel). Note that $\nu_{\max}$ drops sharply at a characteristic field strength ($B_{\max}$), which is a function of both the properties of the grain population and the radial position. The maximum field strength for which perturbations grow in a particular scenario is weaker at larger radii, an effect that is particularly notable when no grains are present. This behaviour results from the instability being (generally) damped when the mid-plane ratio of the Alfvén to sound speed approaches unity (e.g. $v_{\rm A0}/c_{\rm s} \sim 1$; Balbus & Hawley 1991)[2] and the wavelength of the most

[2] Note, however, that perturbations computed in the Hall limit have been found to grow for $v_{\rm A0}/c_{\rm s} \lesssim 3$ (SW03) when the magnetic field is counter-aligned with the disc angular velocity vector ($\boldsymbol{\Omega}$).

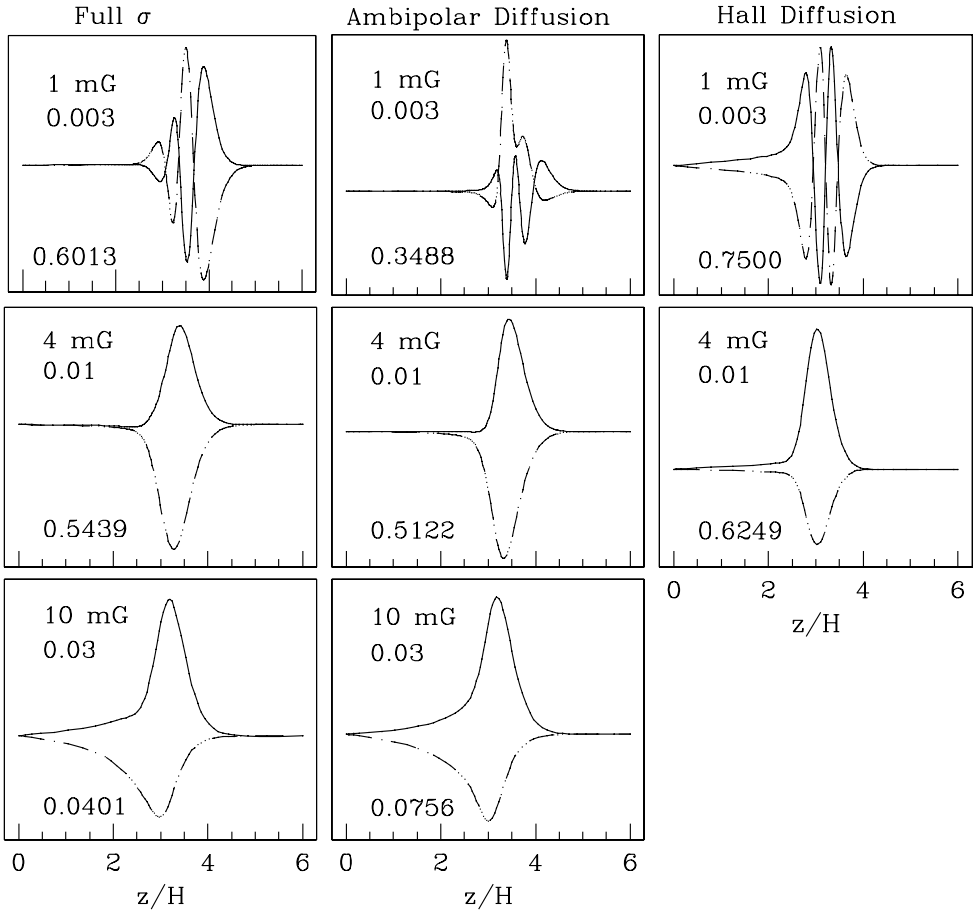


**Figure 9.** Structure and growth rate of the fastest growing MRI modes as a function of height for $R = 10$ au and assuming 0.1 μm grains are present. Different configurations of the diffusivity tensor are shown. The left-hand side column displays solutions incorporating all $\boldsymbol{\eta}$ components ($\eta_A$, $\eta_H$ and $\eta_O$). The middle and right-hand side columns correspond to the ambipolar ($\eta_H = 0$) and Hall diffusion ($\eta_A = 0$) limits, respectively. We find that for relatively weak fields ($B = 1$ and 4 mG), Hall diffusion causes the perturbations to grow faster and closer to the mid-plane than solutions in the ambipolar diffusion limit. For $B =$ 10 mG, the structure of the modes computed with and without the Hall term is fairly similar, as this diffusion mechanism is no longer important at the $z$ where they peak (see bottom panel of Fig. 3).

unstable mode becomes $\sim H$. As the mid-plane density and temperature decrease with radius, the ratio $v_{A0}/c_s$, associated with a particular field strength, increases at larger radii and the perturbations are damped at a weaker field as $r$ increases. Also note that for each radii, the range of field strengths over which unstable modes exist is smaller as the grain size diminishes. This is consistent with the drop in magnetic coupling for a particular field strength as the dust particles are smaller (see Figs 3 and 4).

Finally, note that at 5 au and for weak fields ($B \lesssim 5$ mG, bottom panel of Fig. 11), the MRI grows faster when the small grains are considered than it does in the other scenarios. This is because in this case the modes grow high above the mid-plane, where the magnetic coupling is more favourable, and are completely suppressed at lower $z$. In the other cases, on the contrary, the perturbations grow over a more extended section of the disc and the comparatively low-magnetic coupling closer to the mid-plane reduces their global growth rate. This effect is not so notable at 10 au because of the relatively high-magnetic coupling even at $z = 0$ at this radius.

## 5 DISCUSSION

In this paper, we have examined illustrative examples of the impact of dust grains in the magnetic activity of protoplanetary discs and, in particular, in the linear growth and vertical structure of MRI perturbations. Solutions were computed for $R = 10$ and 5 au assuming a single size grain population of radius $a = 0.1$, 1 or 3 μm, and constituting 1 per cent of the total mass of the gas, is well mixed with the gas phase over the entire vertical extent of the disc. This fraction is independent of height, so we have also assumed that the grains have not sedimented towards the mid-plane. Our results indicate that the perturbations' wavenumber and growth rate are significantly reduced when grains are present. Furthermore, the magnetically inactive – dead – zone, which was practically non-existent when grains were settled, extends to $z/H \sim 3$ at either radii when 0.1 μm-sized grains are considered. At 10 au (5 au), unstable perturbations were found in this case for $B \lesssim 10$ mG (16 mG), a much reduced range compared with the strengths for which they exist when no grains are involved (250 and 795 mG, respectively). This maximum field strength corresponds well to the equipartition field at the height at which the perturbations peak, as expected (e.g. $z/H \approx 3.7$ at 10 au; see lower right-hand panel of Fig. 7).

These results illustrate the impact of dust particles on the dynamics – and evolution – of the weakly ionized inner regions of protoplanetary discs. Solutions at $R = 1$ au are challenging to compute, in particular when the grains are small ($a = 0.1$ μm) and a large section of the disc is expected to remain magnetically

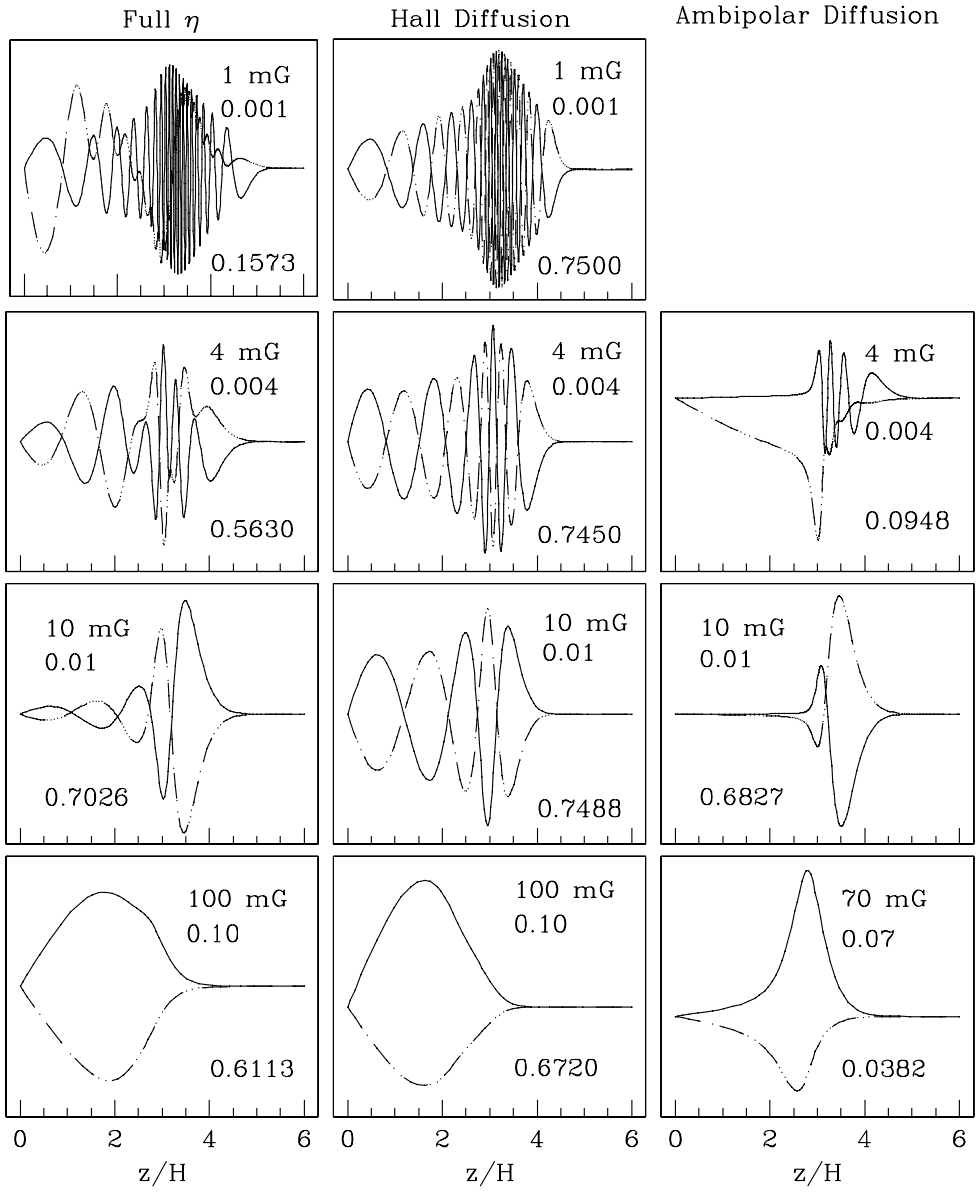


**Figure 10.** Structure and growth of the fastest growing MRI modes as a function of height at $R = 5$ au and assuming 3 μm grains are present. The left-hand side column shows solutions incorporating all $\boldsymbol{\eta}$ components ($\eta_A$, $\eta_H$ and $\eta_O$). The middle and right-hand side columns display the Hall ($\eta_A = 0$) and ambipolar diffusion ($\eta_H = 0$) limits, respectively. Hall diffusion strongly modifies the structure and growth of unstable modes.

inactive (this dead zone extends to ∼2 scaleheights at $R = 5$ au and it is expected to become even larger closer to the star, at least outside the innermost 0.1 au where collisional ionization is effective). However, the solutions presented here can be used to estimate the maximum magnetic field strength to support magnetic activity at that radius. The magnetic coupling at this location, in a disc including 0.1 μm grains, is too weak below $z/H \sim 3.5$ to allow the field to sufficiently couple with the gas (W07). Assuming that the maximum field strength for the MRI to grow is also of the order of the equipartition field at about this height, we can roughly estimate that the MRI should be active for $B \lesssim 400$ mG at 1 au. This is a smaller range than the several gauss for which unstable modes exist when dust grains are not present (SW05). However, MRI modes still grow in this case for a wide range of field strengths.

The results just presented were obtained assuming that the disc surface density profile is that of the minimum-mass solar nebula (MMSN):

$$\Sigma(r) = \Sigma_0 \left(\frac{r}{1\ \mathrm{au}}\right)^{-3/2}, \tag{22}$$

where $\Sigma_0 = 1.7 \times 10^3\,\mathrm{g\,cm^{-2}}$. This implies a surface density of the order of $150\,\mathrm{g\,cm^{-2}}$ at 5 au and $50\,\mathrm{g\,cm^{-2}}$ at 10 au. Recent observational results, however, seem to suggest that the surface density in real discs may drop off more slowly than expected from this model (e.g. Kitamura et al. 2002; Andrews & Williams 2007). More importantly for the analysis presented here, the actual surface densities in the inner regions of protostellar discs ($R < 10$ au) may be smaller than those of the MMSN model [e.g. Andrews & Williams infer a median value of $\Sigma(R = 5\,\mathrm{au})$ of $\sim 14\,\mathrm{g\,cm^{-2}}$, although with considerable scatter]. Inferred values for the outer disc ($R \sim 100$ au and beyond) seem to be in broad agreement with the MMSN (e.g. Kitamura et al. 2002). A smaller surface

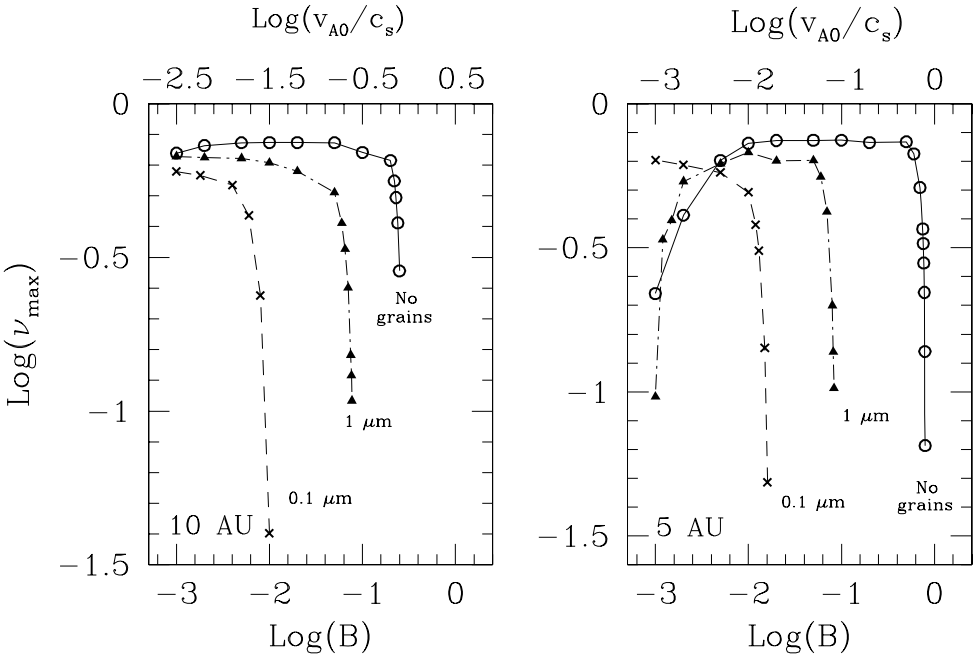


**Figure 11.** Growth rate of the most unstable MRI modes as a function of the strength of the magnetic field for different assumptions regarding the presence, and size, of dust grains mixed with the gas. The solutions are presented for $R = 10$ au (left-hand panel) and $R = 5$ au (right-hand panel).

density will result in ionizing sources (X-rays and cosmic rays) being able to reach deeper into the disc, increasing the ionization fraction of the gas closer to the mid-plane. This effect could, in principle, be strong enough to completely suppress the magnetically dead zone in the disc interior. We also note in this connection, that the possible presence of winds launched centrifugally from the disc surfaces (e.g. BP82; Wardle & Königl 1993), is likely to result in lower column densities – and higher degrees of ionization – than those associated with discs where angular momentum is primarily distributed by the action of the MRI. Semi-analytic models of magnetized accretion discs incorporating both vertical and radial angular momentum transport (via centrifugal winds and MRI-induced turbulence, respectively) seem to suggest that there is a limited opportunity for these mechanisms to coexist over measurable radial extents in real discs (Salmeron, Königl & Wardle 2007). On the other hand, protostellar discs can have surface densities up to ∼50 times higher than the MMSN model before gravitational instability becomes an issue. A more massive disc will result in a more extended section of the disc being shielded from the ionizing fluxes but the coupled column density is unlikely to be drastically affected.

We have also assumed that all grains have the same size and are well mixed with the gas at all $z$. More realistic spatial, and size, distributions must incorporate the effects of dust dynamics and evolution within the disc. Observations of the mid- and far-infrared spectra of discs have provided credible indications that dust properties in discs are indeed different from those of particles in diffuse clouds (e.g. Van Dishoeck 2004; D'Alessio et al. 2006, and references therein). Two aspects of this dust evolution have been clearly identified. First, dust grains coagulate from 0.1 μm to ∼1 mm particles. Secondly, (silicate) material becomes crystallized. It is believed that this crystallization occurs in the disc, given that crystalline silicates are absent from the interstellar medium. Furthermore, the presence of this material at radial locations where the temperature is too low to produce them, suggests significant radial mixing takes place as well (e.g. Van Dishoeck 2004, and references therein). Finally, simulations of dust dynamics and evolution also suggest that in quiescent environments, the grains tend to settle and agglomerate into bigger particles (e.g. Weidenschilling & Cuzzi 1993) and efficiently coagulate and grow icy mantles (Ossenkopf 1993). All these processes modify the surface area of dust grains and impact the recombination rate on their surfaces and the way they drift in response to magnetic stresses. It is also expected that a residual population of small grains would remain (e.g. Nomura & Nakagawa 2006) even when the mean grain size maybe relatively large ($a \gtrsim 1$ μm). This is an important consideration because these small grains tend to carry a significant fraction of the grain charge (W07). The effect of this settling in the spectral energy distribution (and optical appearance) of protostellar discs has been investigated in recent studies (e.g. Dullemond & Dominik 2004).

How quickly, and to what height, dust particles are able to settle is an important, and largely unanswered, question. According to Nakagawa, Nakazawa & Hayashi (1981), the mass fraction of ∼1–10 μm grains mixed well with the gas, diminishes from $\sim 10^{-1}$ to $10^{-4}$ in a time-scale of about $2 \times 10^3$ to $10^5$ yr. Moreover, although the time-scale for dust grains to sediment all the way to the mid-plane may exceed the lifetime of the disc, they may be able to settle within a few scaleheights from the mid-plane in a shorter time-scale (Dullemond & Dominik 2004). This is complicated even more by the expectation that the transition between sections were dust grains is well mixed with the gas, and those completely depleted of them, occurs gradually (Dullemond & Dominik 2004).

MHD turbulence may itself be an important factor for the settling of dust particles. It may, in particular, produce sufficient vertical stirring to prevent settling below a certain height (Dullemond & Dominik 2004; Carballido, Stone & Pringle 2005; Turner et al. 2006). However, this is contingent on the disc being able to generate and sustain MHD turbulence in the vertical sections where the dust is present. This is not guaranteed, even if turbulence exists in other regions, as dust grains efficiently reduce the ionization fraction (and

magnetic coupling) of the gas. As a result, the efficiency – and even the viability – of MHD turbulence in the presence of dust grains, is an important topic that merits careful investigation.

## 6 SUMMARY

We have explored in this paper, the linear growth and vertical structure of MRI-unstable modes at two representative radii ($R = 5$ and 10 au) in protoplanetary discs. Dust grains are assumed to be well mixed with the fluid over the entire section of the disc and, for simplicity, are taken to have the same radius ($a = 3$, 1 or 0.1 μm). They constitute a constant fraction (1 per cent) of the total mass of the gas. These solutions are compared with those arrived at assuming that the grains have settled to the mid-plane of the disc (SW05). We have also explored which disc sections are expected to be magnetically coupled and the dominant diffusion mechanism as a function of height and the strength of the magnetic field, which is initially vertical.

Our models use a minimum-mass solar nebula disc (Hayashi 1981; Hayashi et al. 1985) and incorporate all three diffusion mechanisms between the magnetic field and the neutral gas: Ohmic, Hall and Ambipolar. The diffusivity components are a function of height (as is the density) and are obtained using the method described in W07, to which we refer the reader for details. Essentially, this formalism uses a chemical reaction scheme similar to that of Nishi et al. (1991), but it incorporates higher dust-grain charge states that are likely to occur in discs on account of their larger gas density and temperature in relation to those of molecular clouds. Our calculations also include a realistic ionization profile, with the main ionizing sources being cosmic rays, X-rays and (to a lesser extent) radioactive decay.

Solutions were obtained at the two radii of interest for different grain sizes and configurations of the diffusivity tensor as a function of the magnetic field strength. We refer the reader to SW03 and SW05 for further details of the integration procedure. The main findings of this study are summarized below.

*Magnetic diffusivity*

(i) When no grains are present, or they are $\gtrsim 1$ μm in radius, the mid-plane of the disc remains magnetically coupled for field strengths up to a few gauss at both radii.

(ii) In contrast, when a population of small grains ($a = 0.1$ μm) is mixed with the gas, the section of the disc below $z/H \sim 2$ ($z/H \sim 2.5$) is magnetically inactive at $R = 10$ au (5 au). Only magnetic fields weaker than 25 mG (50 mG) can couple to the gas.

(iii) At 5 au, Ohmic diffusion dominates for $z/H \lesssim 1.2$ when the field is relatively weak ($B \lesssim$ a few milligauss), irrespective of the properties of the grain population. Conversely, at 10 au this diffusion term is unimportant in all the scenarios studied here.

(iv) High above the mid-plane ($z/H \gtrsim 4.5$–5, depending on the specific model), ambipolar diffusion is severe and prevents the field from coupling to the gas for all $B$. This is consistent with previous results by W07.

(v) Hall diffusion is dominant for a wide range of field strengths and grain sizes at both radii (see Figs 3 and 4).

*Magnetorotational instability*

(i) The growth rate, wavenumber and range of magnetic field strengths for which unstable modes exist are all drastically diminished when dust grains are present, particularly when they are small ($a \sim 0.1$ μm; see Figs 7 and 8).

(ii) In all cases that involve dust grains, perturbations that incorporate Hall diffusion grow faster than those obtained under the ambipolar diffusion approximation.

(iii) At 10 au, unstable MRI modes grow for $B \lesssim 80$ mG (10 mG) when the grain size is 1 μm (0.1 μm). This limit [which corresponds to $v_{A0}/c_s = 0.25$ (0.03)] is a much reduced range compared with the $\lesssim$250 mG ($v_{A0}/c_s = 0.8$) for which they exist when ions and electrons are the only charge carriers (SW05). When the grains are relatively large ($a = 1$ and 3 μm), Hall diffusion controls the structure of the modes, which grow even at the mid-plane. In contrast, when the grains are small ($a = 0.1$ μm), the perturbations grow only for $z/H \gtrsim 3$ and are shaped mainly by ambipolar diffusion.

(iv) At 5 au, MRI perturbations exist for $B \lesssim 80$ mG (16 mG) when the grains are 1 μm (0.1 μm) in size [e.g. $v_{A0}/c_s = 0.08$ (0.02)]. For comparison, the upper limit when no grains are present is ∼800 mG ($v_{A0}/c_s = 0.8$; SW05). These modes are shaped largely by ambipolar diffusion, the dominant mechanism at the height where they peak.

The stabilizing effect of small dust grains (e.g. $a = 0.1$ μm) is not strong enough to completely suppress the perturbations. We find, in fact, that the magnetic field is able to couple to the gas and shear over a wide range of fluid conditions even when small dust grains are mixed well with the gas. Despite the low-magnetic coupling, MRI modes grow for an extended range of magnetic field strengths and Hall diffusion largely determines the properties of the perturbations in the inner regions of the disc.

## ACKNOWLEDGMENTS

We thank the referee for useful comments that improved the clarity of the paper. This research has been supported by the Australian Research Council. RS acknowledges partial support from NASA Theoretical Astrophysics Programme Grant NNG04G178G.

## REFERENCES

Andrews S. M., Williams J. P., 2007, ApJ, 659, 705
Balbus S. A., Hawley J. F., 1991, ApJ, 376, 214
Balbus S. A., Hawley J. F., 1998, Rev. Mod. Phys., 70, 1
Blandford R. D., Payne D. G., 1982, MNRAS, 199, 883 (BP82)
Carballido A., Stone J. M., Pringle J. E., 2005, MNRAS, 358, 1055
Consolmagno G. J., Jokipii J. R., 1978, Moon Planets, 19, 253
Cowling T. G., 1957, Magnetohydrodynamics. Interscience, New York
D'Alessio P., Calvet N., Hartmann L., Franco-Hernandez R., Servin H., 2006, ApJ, 638, 314
Dullemond C. P., Dominik C., 2004, A&A, 421, 1075
Fromang S., Terquem C., Balbus S. A., 2002, MNRAS, 329, 18
Gammie C. F., 1996, ApJ, 457, 355
Glassgold A. E., Najita J., Igea J., 1997, ApJ, 480, 344
Glassgold A. E., Feigelson E. D., Montmerle T., 2000, in Mannings V. G., Boss A. P., Russell S., eds, Protostars and Planets IV. Univ. Arizona Press, Tucson, p. 429
Hayashi C., 1981, Prog. Theor. Phys. Suppl., 70, 35
Hayashi C., Nakasawa K., Nakagawa Y., 1985, in Black D. C., Mathews M. S., eds, Protostars and Planets II. Univ. Arizona Press, Tucson, p. 1100
Igea J., Glassgold A. E., 1999, ApJ, 518, 848
Ilgner M., Nelson R. P., 2006, A&A, 445, 223
Johnson E. T., Goodman J., Menou K., 2006, ApJ, 647, 1413
Kitamura Y., Momose M., Yokogawa S., Kawabe R., Tamura M., 2002, ApJ, 581, 357
Königl A., Pudritz R. E., 2000, in Mannings, V. G., Boss, A. P., Russell, S., eds, Protostars and Planets IV. Univ. Arizona Press, Tucson, p. 759

Mathis J. S., Rumpl W., Nordsieck K. H., 1977, ApJ, 217, 425
Matsumura S., Pudritz R. E., 2005, ApJ, 618, L137
Morton D. C., 1974, ApJ, 193, L35
Nakagawa Y., Nakazawa K., Hayashi C., 1981, Icarus, 45, 517
Nakano T., Umebayashi T., 1986, MNRAS, 218, 663
Nishi R., Nakano T., Umebayashi T., 1991, ApJ, 368, 181
Nomura H., Nakagawa Y., 2006, ApJ, 640, 1099
Norman C., Heyvaerts J., 1985, A&A, 147, 247
Oppenheimer M., Dalgarno A., 1974, ApJ, 192, 29
Ossenkopf V., 1993, AA, 280, 617
Salmeron R., Wardle M., 2003, MNRAS, 345, 992 (SW03)
Salmeron R., Wardle M., 2005, MNRAS, 361, 45 (SW05)
Salmeron R., Königl A., Wardle A., 2007, MNRAS, 375, 177
Sano T., Stone J. M., 2002a, ApJ, 570, 314
Sano T., Miyama S., Umebayashi J., Nakano T., 2000, ApJ, 543, 486
Semenov D., Wiebe D., Henning Th., 2006, ApJ, 647, L57
Spitzer L., 1978, Physical Processes in the Interstellar Medium. Wiley, New York
Terquem C., 2003, MNRAS, 341, 1157
Turner N. J., Willacy K., Bryden G., Yorke H. W., 2006, ApJ, 639, 1218
Umebayashi T., Nakano T., 1980, PASJ, 32, 405
Umebayashi T., Nakano T., 1990, MNRAS, 243, 103
Van Dishoeck E. F., 2004, ARA&A, 42, 119
Wardle M., 1997, in Wickramasinghe D., Ferrario L., Bicknell G., eds, Proc. IAU Colloq. 163, Accretion Phenomena and Related Outflows. Astron. Soc. Pac., San Francisco, p. 561
Wardle M., 1999, MNRAS, 307, 849 (W99)
Wardle M., 2007, Ap&SS, 311, 35 (W07)
Wardle M., Königl A., 1993, ApJ, 410, 218
Wardle M., Ng C., 1999, MNRAS, 303, 239
Weidenschilling S. J., Cuzzi J. N., 1993, in Levy E. H., Lunine J. I., eds, Protostars and Planets III. Univ. Arizona Press, Tucson, p. 1031

## APPENDIX A: GOVERNING EQUATIONS

The linearized system of equations that describes the MHD perturbations in the disc is (SW05)

$$i\omega\rho\delta v_{\rm r} - 2\rho\Omega\delta v_\phi - \frac{B_0}{c}\delta J_\phi = 0, \tag{A1}$$

$$i\omega\rho\delta v_\phi + \frac{1}{2}\rho\Omega\delta v_{\rm r} + \frac{B_0}{c}\delta J_{\rm r} = 0, \tag{A2}$$

$$i\omega\delta B_{\rm r} - c\frac{{\rm d}\delta E_\phi}{{\rm d}z} = 0, \tag{A3}$$

$$i\omega\delta B_\phi + c\frac{{\rm d}\delta E_{\rm r}}{{\rm d}z} + \frac{3}{2}\Omega\delta B_{\rm r} = 0, \tag{A4}$$

$$\delta J_{\rm r} = -\frac{c}{4\pi}\frac{{\rm d}\delta B_\phi}{{\rm d}z}, \tag{A5}$$

$$\delta J_\phi = \frac{c}{4\pi}\frac{{\rm d}\delta B_{\rm r}}{{\rm d}z}, \tag{A6}$$

$$\delta J_{\rm r} = \sigma_{\rm P}\delta E'_{\rm r} - \sigma_{\rm H}\delta E'_\phi, \tag{A7}$$

$$\delta J_\phi = \sigma_{\rm H}\delta E'_{\rm r} + \sigma_{\rm P}\delta E'_\phi, \tag{A8}$$

where $\delta E_\phi$ and $\delta E_{\rm r}$ are the perturbations of the electric field in the laboratory frame,

$$\delta E_\phi = \delta E'_\phi + \frac{B_0}{c}\delta v_{\rm r}, \text{ and} \tag{A9}$$

$$\delta E_{\rm r} = \delta E'_{\rm r} - \frac{B_0}{c}\delta v_\phi. \tag{A10}$$

Equations (A1) to (A10) can be expressed in dimensionless form using the following normalization:

$$z^* = \frac{z}{H} \qquad \rho^* = \frac{\rho(r,z)}{\rho_0(r)} \qquad \boldsymbol{\delta B}^* = \frac{\boldsymbol{\delta B}}{B_0}$$

$$\boldsymbol{\delta v}^* = \frac{\boldsymbol{\delta v}}{c_{\rm s}} \qquad \boldsymbol{\delta E}^* = \frac{c\boldsymbol{\delta E}}{c_{\rm s}B_0} \qquad \boldsymbol{\delta E}'^* = \frac{c\boldsymbol{\delta E}'}{c_{\rm s}B_0}$$

$$\boldsymbol{\delta J}^* = \frac{c\boldsymbol{\delta J}}{c_{\rm s}B_0\sigma_\perp} \qquad \boldsymbol{\sigma}^* = \frac{\boldsymbol{\sigma}}{\sigma_\perp}$$

Here, subscript '0' denotes variables at the mid-plane of the disc. Dropping the asterisks, the final system of equations can be expressed as

$$\frac{\rm d}{{\rm d}z}\begin{pmatrix} B_{\rm r} \\ B_\phi \\ E_{\rm r} \\ E_\phi \end{pmatrix} = \begin{pmatrix} 0 & 0 & C_1A_1 & C_1A_2 \\ 0 & 0 & -C_1A_2 & C_1A_3 \\ -\frac{3}{2} & -\nu & 0 & 0 \\ \nu & 0 & 0 & 0 \end{pmatrix}\begin{pmatrix} B_{\rm r} \\ B_\phi \\ E_{\rm r} \\ E_\phi \end{pmatrix} \tag{A11}$$

$$\boldsymbol{\delta J} = C_2\begin{pmatrix} A_2 & -A_3 \\ A_1 & A_2 \end{pmatrix}\boldsymbol{\delta E} \tag{A12}$$

$$\boldsymbol{\delta v} = \chi\frac{1}{1+\nu^2}\begin{pmatrix} -2 & \nu \\ -\nu & -\frac{1}{2} \end{pmatrix}\boldsymbol{\delta J} \tag{A13}$$

$$\boldsymbol{\delta E}' = \frac{1}{\sigma_\perp}\begin{pmatrix} \sigma_{\rm P} & \sigma_{\rm H} \\ -\sigma_{\rm H} & \sigma_{\rm P} \end{pmatrix}\boldsymbol{\delta J}, \tag{A14}$$

where

$$\nu = \frac{i\omega}{\Omega}, \tag{A15}$$

$$C_1 = \chi\left(\frac{v_A}{c_{\rm s}}\right)^{-2}C_2, \tag{A16}$$

$$C_2 = \left[1 + \chi\frac{1}{1+\nu^2}\left(\frac{5}{2}\frac{\sigma_{\rm H}}{\sigma_\perp} + 2\nu\frac{\sigma_{\rm P}}{\sigma_\perp} + \chi\right)\right]^{-1}, \tag{A17}$$

$$A_1 = \frac{\sigma_{\rm H}}{\sigma_\perp} + 2\chi\frac{1}{1+\nu^2}, \tag{A18}$$

$$A_2 = \frac{\sigma_{\rm P}}{\sigma_\perp} + \nu\chi\frac{1}{1+\nu^2}, \text{ and} \tag{A19}$$

$$A_3 = \frac{\sigma_{\rm H}}{\sigma_\perp} + \frac{1}{2}\chi\frac{1}{1+\nu^2}. \tag{A20}$$

This paper has been typeset from a TEX/LATEX file prepared by the author.